ProQuest Number: 10183423

ProQuest 10183423

Wetting of Microstructured Surfaces

Sanaa Aqil

A thesis submitted in partial fulfilment of the requirements of The Nottingham

Trent University for the degree of Doctor of Philosophy

March 2006

Acknowledgment

I would like to thank my supervisor Glen McHale, Mike Newton and Carole Perry for their support and guidance throughout the project.

I would also like to thank Neil Shirtcliffe for his advices and help in the experimental part of this work, as well as my colleagues in the lab: Carl, Dale, Simon, Tristian and the technicians.

I would also like to thank H.Y Erbil for his advices in analyzing drop evaporation data.

Many thanks to Paul Roach.

Lots of thanks to my Family.

And finally Thanks to the Nottingham Trent University for the financial support.

Thank you all

Abstract

This thesis reports a study of the effect of topography on wetting. In the first part of this study the development of a reliable method for producing microstructured patterned SU-8 50 surfaces, using a photolithography technique, is described. These patterns involve tall circular pillars of vertical walls with diameters and spacing that range between 4 and 40 µm, and with aspect ratio (defined as pillars height/pillars diameter) sometimes greater than 4. The contact angle, θ, of water droplets on these patterned surfaces is shown to exceed 150° compared to 80° on the flat surface, dependent on the pattern dimensions; thus surface with wetting tendencies is converted into a non-wetting (hydrophobic) surface as a consequence only of surface topography variation. Subsequently these patterned surfaces were used to study the dynamics of spreading of drops of a non-volatile viscous polydimethylsiloxane (PDMS) oil, which spreads completely on a flat SU-8 surface. The exponent, n, of the power law of the dynamic contact angle-time relation $\theta \propto t^{-n}$ is shown to increase from 0.3 on a flat towards 0.75 on surfaces of very tall pillars. The pattern is also shown to convert the drop edge speed, v_e, from a cubic function in the dynamic contact angle, $v_e \propto \theta^3$, towards a linear function, $v_e \propto \theta$.

In the final part of this thesis, qualitative and quantitative features of the evaporation of water droplets with initial contact angles of ~ 130° -150°are described. Both pinned contact area and retreating contact line evaporation were observed corresponding to droplets in initial states of either Wenzel or Cassie states (i. e. penetrating surface features or suspended upon them). For droplets beginning in the Cassie state, a transition to the Wenzel state was observed. A model for the constant contact area mode of evaporation was applied to the data and a diffusion coefficient of water vapour into the surrounding air ((2.6 ± 0.2)x10^{-5} m^{2}s^{-1}) was obtained consistent with reference literature to within 8%.

Table of contents

List of Figures

hydrophobicity ($90<\theta_e<\theta_c$). For very hydrophobic material $\theta_e > \theta_c$ the Cassie model should be selected. [Ref. 17]

Figure 4.4. Scanning electron microscope image of electrodeposited surface. The sample is tilted to70°.

Figure 4.5. A droplet of water on a surface produced by electro-deposition

Figure 4.6. A droplet of water contact angle of 153 obtained on a patterned surface of diameter-separation-height measured to be 11.5, 18.5, 25 μm respectively.

Figure 4.7. The right hand side of this figure presents Cassie model (a drop suspended on pillars). The left hand side may be the real shape of the drop base, where a curvature is developed in the gaps of the pattern. This partial penetration could be due to the drop weight or because the pattern acts as a connected capillary tubes. From a theoretical point of view no penetration is possible if the pattern is in the from of isolated capillary tubes.

Figure 4.8. Water contact angle on patterned surface with different heights. (a) unhydrophobized (b) hydrophobized. Ref. [1].

Figure 4.9. Angle versus time curves for the flat (▲) and a structured surface (■) with pillar diameter of 15 μm and height of 26 μm.

Figure 4.10. The measured and calculated dynamic contact angle-time relationship on a log-log scale for the structural surface with pillar diameter of 15 μm and height of 26 μm; the volume variation with time is also plotted.

Figure 4.11. The measured and calculated drop base diameter-time relationship on a log-log scale for the structural surface with pillar diameter of 15 μm and height of 26 μm; the volume variation with time is also plotted.

Figure 4.12. The edge velocity-dynamic contact angle relationship on a log-log scale for the smooth and a structured surface. The diameter-separation – height are 15, 15 and 26 μm respectively.

Figure 4.13. Exponent p extracted from the edge speed-dynamic contact angle (xxx) for spreading of PDMS on patterned surfaces; the dotted curve indicates the trend from cubic to linear form. The variation of the dynamic contact angle-time exponent n (ooo) with pillar height is indicated by the right hand axis [12].

Figure 4.14. The precursor film (moving to the left) seems to be attracted to the pillars, probably indicating superspreading driven by surface structure.

Figure 5.1. Evolution with time of the contact angle (♦♦♦) contact diameter (□□□) and height (▲▲▲) during droplet evaporation from flat surface.

Figure 5.2. Evolution with time of the contact angle (♦♦♦) contact diameter (▲▲▲) and height (□□□) during droplet evaporation from Cassie surface.

Figure 5.3. Evolution with time of the contact angle (♦♦♦) contact diameter (□□□) during the step wise retreat for a droplet evaporating from Cassie surface.

Figure 5.4. Evolution with time of the contact angle (♦♦♦) contact diameter (□□□) and height (▲▲▲) during droplet evaporation from Wenzel surface. Evolution

Figure 5.5. A Wenzel drop late in the evaporation. The drop contact angle decrease from e to h while the contact diameter remains pinned as the drop volume decrease.

Figure 5.6. Drop evaporating from flat surface. Both of the contact angle and contact diameter decrease as the drop volume decrease from a to d.

Figure 5.7. Transition from Cassie to Wenzel can occur either in the middle of the evaporation process (c to d present drop collapse in one frame) or late in the evaporation (g to h).

Figure 5.8. Evolution with time of the contact angle (♦♦♦) contact diameter (□□□) and height (▲▲▲) during droplet evaporation . The data corresponds to figure 5.7, a to d.

Figure 5.9. Tests of equation (5.1) and equation (5.2) for the data in figure (5.2) (lower pairs of curves), figure (5.4) (middle pair of curves) and figure (5.6) (upper pair of curves). The solid lines are fits over the range to when the drop contact angle becomes 90 (upper pair), collapse (middle pair) or start the stepwise retreat (lower pair). The data of the upper pair of curves was multiplied by 1.5 to avoid intersection with the middle pair curves data.

List of tables

Chapter 1

Introduction

1.1 Introduction

Wetting is defined as the extent to which a liquid spreads over a surface. A drop of liquid may spread over the surface to form a thin film or form a drop with finite contact angle. The former regime is called complete wetting, while the latter is called partial wetting. The tendency of liquids to choose between the two regimes is a function of the various surface tension forces between the three interface surfaces (solid-vapour, solid-liquid and liquid-vapour) in the system. Wetting is encountered in everyday life; fluids tend to wet surfaces and stick to them. One example is a rain drop stuck to a window, where the surface tension forces counteract the force of gravity and prevent the drop from falling.

Understanding how drops sit on a solid surface and how they spread out to form a thin film is needed for control and manipulation of liquids on surfaces. This is relevant to many applications such as self cleaning glass, guided motion of drops in microfluidic devices, DNA analysis and spotting and other [1]. The idea of surface manipulation attracted world wide interest after the spectacular achievement of superhydrophobic surfaces with a water drop contact angle of 174° [2]. This type of hydrophobicity is observed in nature on Lotus leaves [3], where a microstructure found on the leaves leads to the self-cleaning property of this plant. Mimicking such a property is possible by (for example) creating double (multiple) roughness structure, in which a surface structure can be created on a rough or structured surface. Mimicking such a

property on solid surfaces becomes an objective of many materials oriented researches, and was achieved by various groups. One of them is Patankar *et al* who achieved self cleaning surface by creating a double (or multiple) roughness structure [4].

This study follows the theme of wetting and surface roughness. The originality is that it investigates the wetting and non wetting behaviour on idealized microstructured superhydrophobic surfaces as well as the effect of varying the surface structure dimensions, going beyond static wetting conditions to investigate mechanisms related to wetting such as spontaneous spreading and evaporation. Spreading is relevant to many industrial applications like coating, printing, and painting, while evaporation is relevant to heat and mass transfer processes.

Well-ordered microstructured surfaces created using a photolithography technique were used to obtain the superhydrophobic behaviour and to also study the spreading of polydimethylesiloxane (PDMS) oil and the evaporation of water. The study provides a description of droplets dynamic behaviour as well as quantitative formulas for spreading speed and water diffusion coefficient. The overall goal of this thesis is a better understanding of wetting phenomena on microstructured surfaces, which may lead to better control of the surface wetting applications.

1.2   Aims and summary of the project

The general aim of this work is to study the wettability of well-defined patterned surfaces.

The first aim was to produce patterned surfaces with high aspect ratio. This was done by developing a photolithography technique using thin film techniques. Patterned surfaces consist of circular pillars of diameter ranging between 4 and 20 µm and separated by distances ranging from 4 to 20 µm were obtained [5]. The highest aspect ratio obtained using photolithography was greater than 4.

The second aim was to study the static wetting through contact angle measurement of water droplets on these patterned surfaces of various dimensions. One sample pattern (of diameter equal to separation and both equal to 15 µm) was chosen to characterize the hydrophobicity of the surfaces as a function of pillars height (or roughness factor). The highest contact angle obtained on that sample pattern was ~143° instead of ~80° for water droplets on the flat surface [5]. Contact angles of greater than 150° were obtained on other patterned surfaces of smaller diameter and larger separation between the pillars (153° was obtained on a surface of diameter equal to 10 µm and separation equal to 20 µm).

The third aim was to confirm experimentally that the surface topography increases the speed of the spreading. This was done by following the evolution with time of the profile of polydimethylsiloxane (PDMS) oil droplets'

on the microstructured patterned surfaces, which is known to achieve complete wetting on flat surfaces. The droplets' edge speed-dynamic contact angle relation for spreading on patterned surfaces is compared with those of droplet spreading on flat surfaces. The patterned surfaces were shown to enhance the drop spreading of a completely wetting liquid [6].

The fourth aim was to study the influence of the surface structure on the evaporation pattern and to estimate the diffusion coefficient of water vapour into the air. A description of the evaporation process from these microstructured patterned surfaces plus an estimate of the product of diffusion coefficient and concentration difference from the evolution of droplet profile with time were obtained. [7]

1.3 Literature review

1.3.1 Young's equation

The oldest theory of wetting is that by Young in 1805, which he expressed in words only [8] but later translated into the language of mathematics as

$$\cos\theta = \frac{\gamma_{sv} - \gamma_{sl}}{\gamma_{lv}} \tag{1.1}$$

where θ (figure 1.1) is the contact angle, and is geometrically defined as the angle formed by the intersection of the two planes tangent to the liquid and solid surfaces at the perimeter of contact between the two phases and the third surrounding phase, which will be air or vapour [9]; γ_{SV}, γ_{SL} and γ_{LV} are the solid-vapour, solid-liquid and liquid-vapour interfacial tensions, respectively.
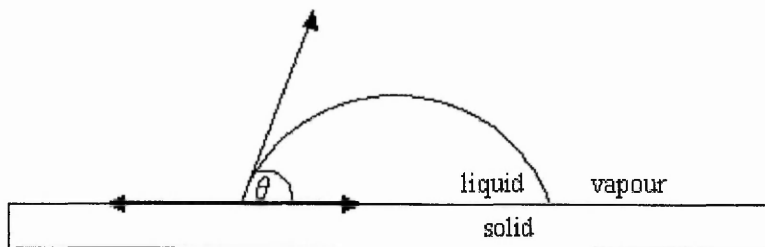
Figure 1.1. A schematic representation of the contact angle θ.

If the contact angle is less than 90°, the system is said to have a tendency to wetting, while if the contact angle is greater than 90°, then the system has a tendency to non- wetting. The equation later became the basis for many studies of wetting.

1.3.2 Contact angle and surface heterogeneities

In 1936 Wenzel [10] studied the effect of surface roughness on the contact angle; he suggested that roughness modifies the cosine of the contact angle by a factor r, which represents the ratio of the actual area of the solid-liquid contact to the projected area on the horizontal plane. Unlike Wenzel, Cassie and Baxter (in 1945) postulated that the cosine of the contact angle of a liquid drop on a heterogeneous surface was equal to the sum of the cosines of the contact angles on the homogeneous surfaces of the respective materials, weighted by the amount of the available surface [11]. On the basis of Wenzel and Cassie-Baxter models for the contact angle on a rough surface, many studies have appeared. Since 1996, the creation of super hydrophobic (highly non-wetting) surfaces with contact angles greater than 150 ^{o} has been of world-wide interest. This interest was initiated by Onda *et al* [2] who obtained a surface using a paper-sizing agent that gave a contact angle for water of 174°. Other researchers have designed surfaces with water contact angles greater than 150°, examples include vacuum deposited PTFE thin films [12], anodic oxidation of aluminium surfaces [13,14], porous surfaces made by the sol-gel process [15], glass beads surfaces [16], plasma polymerization [17,18], and lithographic patterning of silicon wafers [5,19,20].

A water drop rolls easily on these rough surfaces picking up with it any dust particles and so results in a self-cleaning mechanism. Blossey (in 2003) published an article reviewing a number of ways to produce these

superhydrophobic surfaces and the problems facing this industry, which he attributed to aging and decay [1].

1.3.3 Surface heterogeneity and hysteresis

The contact angle measured for a liquid advancing across a surface exceeds that of one receding from the surface. This difference, known as contact angle hysteresis, can be quite large, as much as 50 $^{\circ}$ for water on mineral surfaces [21]. Researchers attribute it to many causes. The best known causes are surface roughness and chemical heterogeneities [21-24]. This is because physical or chemical heterogeneities of the surface cause differences in the surface free energy from point to point along the contact line, and therefore in the contact angle. Other causes include solution impurities adsorbed on the surface, alteration of the surface by solvent [22] and possibly drop size effect [25,26].

To avoid hysteresis the contact angle measurement has to be carried out on a smooth surface in ideal and clean conditions. Any deviation from the ideal condition can lead to a serious error. A quantitative measurement of the effect of surface roughness on the advancing and receding contact angles was carried out by Dettre and Johnson [23] in 1964 who conducted a number of experiments on chemically patterned surfaces created by different patches of surfaces. Their conclusion was that hysteresis increases with roughness. Figure 1.2 shows their results.
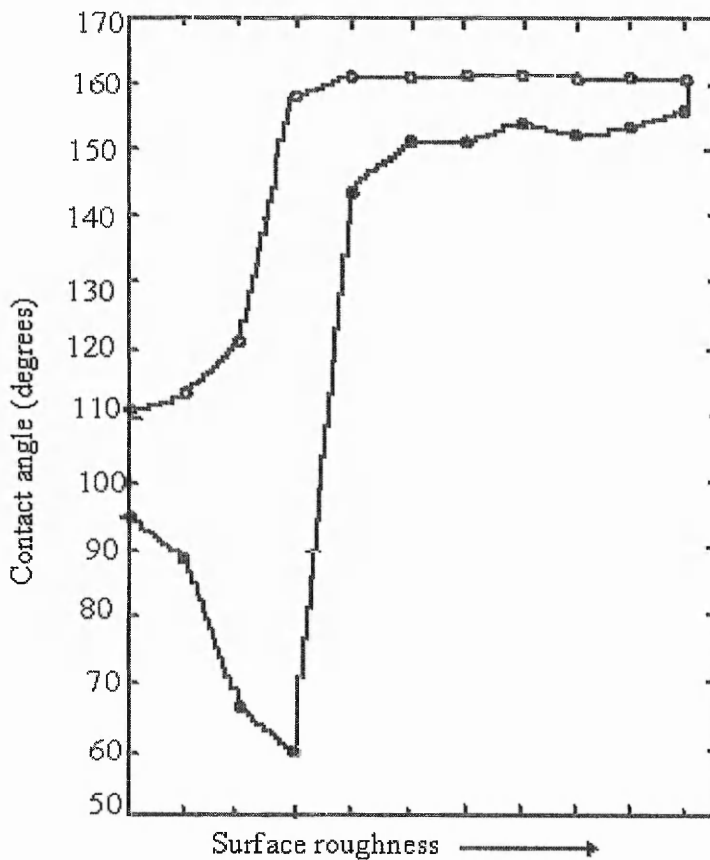
Figure 1.2. Advancing (open symbols) and receding (closed symbols) contact angles of water on a wax surface as a function of the surface roughness. The roughness of the wax surface was varied by repeating a number of successive heat treatments of the wax [Ref. 23].

Many publications have appeared in the last few years trying to shed more light on the relation between surface heterogeneities and contact angle [27-36]. It has been suggested that the cause of hysteresis on a heterogeneous surface is that it permits the existence of a large number of metastable states [24]. Recent studies on hysteresis support this hypothesis [27,28]. Patanker

[27] showed that on a rough hydrophobic surface, two possible drop configurations are possible, depending on how the drop is formed (or the available energy during deposition). The first corresponds to Wenzel state, where the drop wet the grooves, and the second corresponds to Cassie, with the drop sitting on a composite surface made of roughness peaks, and air. The experimental data of Junghon Lee *et al* [28] confirm this, and suggest a possible transition between the two states by an external disturbance. The Cassie state shows much less hysteresis than the Wenzel. Less hysteresis means less resistance to flow and therefore it has a potential for applications involving moving drops on open surfaces or microchannels [34]. Quéré refers to Cassie type as slippery surfaces and to the Wenzel state as sticky surfaces [29]. Potential applications of these surfaces were presented by McHale *et al* [36].

1.3.4 Wetting and spreading

The spreading of liquids on solid surfaces is a very important process in coating technologies with relevance to lubrication, adhesion, spraying, painting, printing, biological cell adhesion and others. Therefore a fundamental understanding of the spreading mechanism is essential for process control. The modelling of drop spreading has been dealt with in the literature using two theoretical approaches i) fluid dynamics and ii) molecular kinetic energy approach.

Among those who dealt with the drop spreading from a fluid hydrodynamics point of view is Tanner [37], who studied the spreading of droplets of a viscous

liquid on a smooth surface. He solved the hydrodynamic equation (for a drop spreading on a smooth homogeneous surface) assuming that the only driving force is capillarity and concluded that the spreading of small non-volatile drops spreading on a complete wetting surface (i.e. ones with vanishing equilibrium contact angles) follows a power law in time, $\theta \sim t^{-3/10}$ and $d \sim t^{1/10}$ where θ and d are the dynamic contact angle and the drop base diameter respectively. The chemical nature of the surface seems to play no further role in the dynamics of the spreading mechanism once the surface becomes complete wetting. A number of researchers subsequently confirmed that the variation of base diameter with time follows $d \sim t^{1/10}$ in the early stages of the spreading process where the main driving force is the Laplace pressure, but when the curvature of the liquid surface become small, then the gravity is the main driving force [22], and the relation changes to $d \sim t^{1/8}$ [38]. The relation between the drop edge velocity and the dynamic contact angle was given by Hoffman in 1974 as $v_e \sim \theta^3$ [39]. Tanner reached the same conclusion in 1979 when he performed a number of experiments using silicone oils [37]. The relation was again confirmed by De Gennes in 1985 [22].

The drop spreading is preceded by a microscopic film known as the precursor film. It was first observed by Hardy in 1919 [40] and then reported by many research groups [22,42,43,44]. This film is caused by the van der Waals attraction between the solid and the liquid and is present in both the moist and dry spreading. It is caused by vapour condensation on the solid during volatile liquid spreading, whilst during non-volatile liquid spreading case; it is formed

by the liquid flow [43, 44]. When the volume of the liquid involved in this film is non negligible compared to the total volume of the drop, the macroscopic kinetics departs from Tanners law [45], which assumes constant volume, and the spreading is then affected by the van der Waals forces (ignored by Tanner) and in this case it has been suggested to use the molecular kinetic approach in dealing with such a spreading [22,46].

The crossover from Tanner spreading regime to the spreading dominated by van der Waals was discussed by Stiener *et al* [47] who studied the spreading of polydimethylsiloxane drops on substrates of various surface energies and concluded that the drop volume determines the spreading regime.

The previous spreading studies were performed on (approximately) smooth surfaces. Cox [48] studied the spreading on rough surfaces (parallel grooved surfaces). He found that when the contact line is parallel to the groove, the macroscopic contact angle would oscillate by an amount of order ε (where ε is the characteristic slope of the surface roughness) and expected stick-jump behaviour of the contact line. McHale and Newton [49] also developed a model of dynamic wetting on rough surfaces. They applied Frenkels' method [49,50] to derive a time dependence relation of the dynamic contact angle as well as a relation between the drop edge velocity and the dynamic contact angle for both chemically and physically heterogeneous surfaces. They predicted that when surface roughness is strong the dynamic contact angle tends to be proportional to $t^{-3/4}$, and the edge velocity tends to a linear function

of the dynamic contact angle ($v_e \propto \theta$). Experimental investigation and verification of their prediction using drops of silicone oil spreading on structured surfaces forms part of this thesis. Both the technique for creating these surfaces and the studies of power law dynamics have been published [5,6].

1.3.5 Wetting and evaporation

The influence of surface wetting on the evaporation process has been studied by various investigators. Picknett and Bexon [51] studied the evaporation of organic drops of liquid on a nearly flat surface, where they measured the loss of mass and the drop profile at intervals. They reported 3 modes of evaporation, mode 1 corresponding to a constant solid-liquid contact area; mode 2, corresponding to constant contact angle, and mode 3, corresponding to changes in both contact angle and contact area. They also developed a diffusion based theory to predict the evaporation rate.

Birdi, Vu and Winter [52] followed the evaporation of water, and n-octane drops on glass and Teflon surfaces respectively, where they measured the mass loss as a function of time. They concluded that for much of the time, the evaporation rate is linear and is proportional to the drop contact radius. In a subsequent paper Birdi and Vu concluded that the linearity of evaporation rate in time is only for $\theta < 90°$ [53].

Rowan *et al* [54,55] also studied the evaporation of water on poly methyl methacrylate (PMMA) surfaces and of three alcohols (of initial contact angle less than 90°) on Teflon surfaces. They concluded that the evaporation is dominated by an initial stage with constant contact radius. The contact radius then decreases causing instability of the contact angle, which they attributed to the surface tension driven flow due to evaporative cooling.

Bourges and Shanahan [56] considered the evaporation of droplets of water from smooth polyethylene and both smooth and rough epoxy resin surfaces. They obtained a measurement of height, contact angle and contact radius as a function of time. They found that evaporation consists of three or four distinct stages, depending on the surface roughness. For the constant solid - liquid contact area, they developed a model for calculating the diffusion coefficient of water vapour into the air.

McHale *et al* [57] studied the evaporation of water drops from PTFE (non-wetting) surface, where the initial contact angle was 112°. They noted that the contact angle remain constant (about 108°) for the majority of the evaporation time, which they attributed to the local saturation of the vapour in the region of the contact line and low contact angle hysteresis. They developed a diffusion model for the various geometrical factors and time for the non-wetting system assuming constant contact angle, which then provided an estimate for the diffusion coefficient.

Erbil *et al* [58] compared the different methods in literature for estimating the diffusion coefficient of water vapour into the air from the drop evolution data with time and concluded that the Picknett and Bexon model gave the best fit. Surface wetting could be varied by using different liquids or mixture. Sefiane *et al* [59] studied the evaporation of water-ethanol mixtures, where they varied the ethanol concentration (which results in variation of the initial contact angle). They concluded that the dynamic contact angle is highly dependent on the concentration of the more volatile component. At high ethanol concentration (in the beginning of the evaporation) the contact angle of the drop matches the behaviour of pure ethanol, while toward the end of the drop life time the contact angle jumps to a higher value and follows the behaviour of the pure water.

In this study the evaporation of small water droplets is investigated. Unlike all the publications mentioned earlier (in the area of wetting and evaporation) the initial contact angle was higher than 120°, sometimes as high as 153°. These results on evaporation from superhydrophobic surfaces have been published [7].

1.4   Project overview

In the following chapters a theoretical background of the wetting studies is given, followed by description of the experiments used in studying wetting on patterned surfaces, as well as results and discussions.

Chapter 2 is a theoretical background of static and dynamic wetting. It first explains the forces affecting a drop on solid surface in static condition and defines the contact angle and hysteresis and explains methods of measuring the static contact angle. Then it presents models of drop configuration on rough hydrophobic surface (Wenzel and Cassie). The wetting dynamic part explains the forces driven drop spreading. The main driving force in the experiments performed in this work (capillarity), and the influence of surface roughness on spreading are discussed. The last part of the theory chapter talks about wetting and evaporation since evaporation causes changes in drops' contact angle and base diameter, and present a method for calculating the diffusion constant of water molecule into the surrounding atmosphere.

Chapter 3 is the experimental part of this work. It gives a description of techniques, equipments and experimental setups used. This includes description of the fabrication process of microstructured patterned surfaces using a photolithography technique as well as rough surface fabrication using electrodeposition. The characterization of these surfaces was done using scanning electron microscopy or confocal microscopy and contact angle

measurement, which are all described. Experimental setup for following drop spreading and evaporation processes using the Kruss system to insure that the drop is in the appropriate position during motion are also described in this chapter.

Chapter 4 and 5 present results obtained from the experiments performed, and discuss whether the results are consistent with the theoretical predictions. Chapter 4 begins by presenting good and bad samples of microstructured patterned surfaces obtained by photolithography with explanation of the causes of bad surface results. A sample of rough surface produced by electrodeposition is also presented. The hydrophobicity of a sample pattern (15 μm in diameter pillars separated by 15μm and arranged in a square lattice) is presented as a function of pillars height. Results from spreading experiment of PDMS oil droplets on these microstructured surfaces are presented and compared with the spreading of PDMS oil droplets on flat surfaces. Chapter 5 present results obtained from analyzing the recorded process of small water drops evaporation. The two distinct manner of evaporation (Wenzel and Cassie drop) are discussed and the differences between the two cases are mentioned. Calculation of the water diffusion constant is also presented and discussed.

The conclusion and possible future work are found in Chapter 6.

References

1. R. Blossey, *Nature Materials*, 2, **2003**, 301.

2. T. Onda, S. Shibuichi, N. Satoh, K. Tsujii, *Langmuir*, 12, **1996**, 2125.

3. W. Barthlott, C. Neinhuis, *Planta*, 202, **1997**, 1.

4. N. A. Patankar, *Langmuir*, 20, **2004**, 8209.

5. N. J. Schirtcliffe, S. Aqil, C. Evans, G. McHale, M. I. Newton, C. C. Perry, P. Roach, *Journal of Micromechanics and Microengineering*, 14, **2004**, 1384.

6. G. McHale, N. J. Shirtcliffe, S. Aqil, C. C. Perry, M. I. Newton, *Physical Review Letters*, 93, **2004**, article 036103.

7. G. McHale, S. Aqil, N. J. Shirtcliffe, M. I. Newton, H. Y. Erbil, *Langmuir*, 21, **2005**, 11053.

8. J. J. Bikerman, Physical surfaces, *Academic press*, **1970**, chapter 6, p. 239.

9. D. Myers, Surfaces, Interfaces and Colloids Principles and Application, *VCH Publisher*, **1991**, chapter 17, p. 351.

10. R. N Wenzel, *Industrial Engineering Chemistry*, 28, **1936**, 988.

11. A. B. D. Cassie, S. Baxter, *Transaction of Faraday Society*, 40, **1944**, 546.

12. J. D. Miller, J. Veeramasuneni, J. Drelich, M. R. Yalamanchili, *Polymers Engineering Science*, 36, **1996**, 1849.

13. S. Shibuichi, T. Yamamoto, T. Onda, K. Tsujii, *Journal of Physical Chemistry*, 100, **1996**, 19512.

14. S. Shibuichi, T. Yamamoto, T. Onda, K. Tsujii, *Journal of Colloids and Interface Science*, 208, **1998**, 287.

15. K. Tadanaga, J. Morinaga, T. Minami, *Journal of Sol Gel Science and Technology*, 19, **2000**, 211.

16. M. Fuji, H. Fujimori, T. Takei, T. Watanabe, M. Chikazawa, *Journal of Physical Chemistry B*, 102, **1998**, 10498.

17. W. Chen, A. Y. Fadeev, M. C. Hsieh, D. Öner, J. P. Youngblood, T. J. McCarthy, *Langumir*, 15, **1999**, 3395.

18. S. R. Coulson, I. Woodward, J. P. S. Badyal, S. A. Brewer, C. Willis, *Journal of Physical Chemistry B*, 104, **2000**, 883.

19. D. Quere, D. Richard, *Europhysics Letters*, 48, **1999**, 286.

20. D. Oner and T. J. McCarthy, *Langmuir*, 16, **2000**, 7777.

21. A.W. Adamson, A. P. Gast, Physical Chemistry of Surfaces, sixth edition, *Wiley,* **1997**.

22. P. G. de Gennes, *Review of Modern Physics,* 57, **1985**, 827.

23. R. E. Johnson, R. H. Dettre, *Advancement in Chemistry Series*, 43, **1964**, 12.

24. E. Rulon, J. R. Johnson, R. H. Dettre, *The Journal of Physical Chemistry*, **1964**, 1744.

25. S. Branden, N. Haimovich, E Yeger, A. Murmur, *Journal of Colloid and Interface Science*, 263, **2003**, 237.

26. J. Gaydos, A. W. Neumann, *Journal of Colloid and Interface Science*, 120, 1, **1987**, 76.

27. N. A. Patankar, *Langmuir*, 19, **2003**, 1249.

28. J. Lee, N. A. Patankar, B. He, *Langmuir*, 19, **2003**, 4999.

29. D. Quere, A. Lafuma, J. Bico, *Nanotechnology,* 14, **2003**, 1109.

30. A. Lafuma, D. Quere, *Nature*, **2003**, 457.

31. C. W. Extrand, *Langmuir*, 18, **2002**, 7991.

32. W. Extrand, *Journal of Colloid and Interface Science*, 248, **2002**, 136.

33. T. S. Meiron, A. Murmur, I. S. Saguy, *Journal of Colloid and Interface Science*, 274, **2004**, 637.

34. J. Kim and C-J Kim, *The 15th IEEE International Conference*, **2002**, 52.

35. C. Cottin-Bizonne, J. L. Barrat, L. E Bocquet, E. Charlaix , *Nature*, **2003**, 237.

36. G. McHale, N. J. Shirtcliffe, M. I. Newton, *Analyst*, 129, **2004**, 284.

37. L. H. Tanner, *Journal of Physics: Applied Physics*, 12, **1979**, 1473.

38. S. Gerdes, A. M. Cazabat, G. Strom and F. Tiberg, *Langmuir*, 14, **1998**, 7052

39. R. Hoffman, *Journal of Colloid and Interface Science*, 50, **1975**, 228.

40. P. G. De Gennes, The (**1994**) Dirac Memorial Lecture, *Cambridge University press*.

41. S. Gerdes, A. M. Cazabat, G. Strom, *Langmuir*, 13, **1997**, 7258.

42. F. Helsot, A. M. Cazabat, N. Fraysse, P. Levinson, *Advances in Colloid and Interface Science*, 39, **1992**, 129.

43. D. Aussere, A. M. Picard and L. leger, *Physical Review Letters,* 57, **1986**, 2671.

44. L. Leger, A. M. Guinet-Picard, D. Ausserre. And C. Strazielle, *Physical Review Letter*, 60, **1988**, 2390.

45. P. Siberzan, L. Leger, *Physical Review Letter*, 66, **1991**, 185.

46. L. M. Hocking, *Physics of Fluids*, 10, **1994**, 3224.

47. E. Perez, E. Schffer and U. Stiener, *Journal of Colloid and Interface Science*, 234, **2001**, 178.

48. R. G. Cox, *Journal of Fluid Mechanics*, 131, **1983**, 1.

49. G. McHale, M. I. Newton, *Colloids and Surfaces (A)*, 206 (**2002**), 193.

50. J. Frenkel, *Journal of physics, USSR*, 9, **1945**, 385.

51. R. G. Picknett, R. J. Bexon, *Journal of Colloid Interface Science*, 61, **1977**, 336.

52. K. S. Birdi, D. T. Vu, A. J. Winter, *Physical Chemistry*, 93, **1989**, 3702.

53. K. S. Birdi, D. T. Vu, *Journal of Adhesion Science Technology*, 7, 1993, 485.

54. S. M. Rowan, M. I. Newton, G. McHale, *Journal of Physical Chemistry*, 99, **1995**, 13268.

55. S. M. Rowan, G. McHale, M. I. Newton, M. Toorneman, *Journal of Physical Chemistry*, 101, **1997**, 1265.

56. C. Bourgès-Monnier, M. E. R. Shanahan, *Langmuir*, 11, **1995**, 282.

57. G. McHale, S. M. Rowan, M. I. Newton, M. K. Banerjee, *Journal of Physical Chemistry B*, 102, **1998**, 1964.

58. H. Y. Erbil, G. McHale, M. I. Newton, *Langmuir*, 18, 2002, 2636.

59. K. Sefiane, L. Tadrist, M. Douglas, *International Journal of Heat and Mass Transfer*, 46, **2003**, 4527.

Chapter 2

Theory

2.1 Introduction

This chapter presents an overview of the theoretical background required for a practical understanding of the work in this thesis. It defines and explains physical terminology used in this thesis, such as surface tension, surface free energy, capillarity, contact angle, wetting and wetting hysteresis. It also explains the effect of surface roughness on the contact angle (Wenzel and Cassie models).   Causes of drop spreading are explained with special attention given to the spreading of non volatile viscous liquids on rough solid surfaces. A model for the evaporation of water droplets based on the diffusion of water molecules into the surrounding atmosphere is given, as well as equations for calculating the diffusion constant-vapour concentration difference product ($D\Delta c$) from the data of evolution of drop profile with time.

2.2 Surface Tension

When a liquid is placed in a solid container, the attraction between the liquid around the edge and the adjacent solid molecules causes the liquid meniscus to curve. Such a curvature is caused by the surface tension force which arises from the forces between the molecules of a liquid and the forces between the liquid molecules and those of any adjacent substance. The same force is responsible for the rise (or depression) of liquid in capillary tubes as well as the formation of smooth drops.

Surface tension force may be defined as a contractile force, which tends to shrink the surface, and acts perpendicular and inward from the boundaries of the surface, operating around the perimeter of the surface. This tension originates from the unbalanced force on the molecules at the surface. The liquid behaves as if it had a skin that prevents it, up to a point, from overflowing. All phases' boundaries behave this way, not just liquid surfaces; however the evidence for this is more apparent for deformable liquid surfaces [1]. Surface tension (denoted by γ_{LV} where the subscript LV refers to the liquid-vapour) is a force per unit length; however it is sometimes referred to as a surface tension force which is also equal to surface free energy per unit area. Table 1 [2] gives liquid-vapour surface tension (γ_{LV}) data of some common liquids at 25°C, the unit is milli- Newton/meter (mN m^{-1}).

Molecular formula	Liquid	Liquid-vapour surface tension γ_{LV} (mN/m)
Hg	Mercury	485.48
H_2O	Water	71.99
$C_{10}H_{22}$	Decane	23.37
C_2H_6O	Ethanol	21.97
C_8H_{18}	Octane	21.14

Table 2.1. Surface tension of some liquids at 25°C

2.3 Surface free energy

Consider 2 molecules (figure 2.1), B in the bulk and A at the surface, the line MN indicate the boundaries between the liquid and the vapour phase. The net force on the particle B is zero because of the symmetry inside the bulk fluid. On the other hand, the molecule A is attracted by the liquid more than by the vapour. To bring a molecule from the inside to the surface, work must be exerted to overcome the surface tension force (to overcome the net inward attraction by the fluid). The results of extending the surface area is what is called the surface free energy and thus defined as the work spent on moving molecules from the bulk to the interface [3].

Vapour

M   A   N

Liquid

B
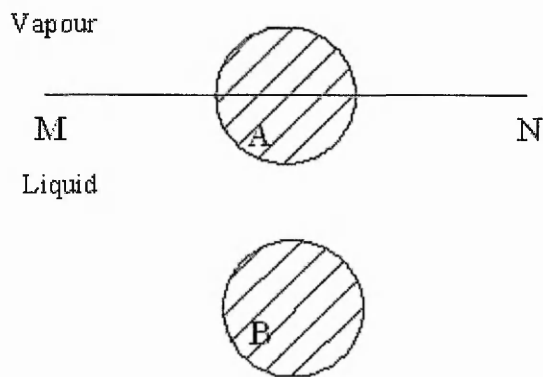
Figure 2.1. Two molecules in a liquid A is at the surface and B is in the bulk.

When the liquid encounters another substance, there is usually an attraction between the two materials. The adhesive forces between the liquid and the second substance will compete against the cohesive forces of the liquid. Liquids with weak cohesive bonds and a strong attraction to another material (or the desire to create adhesive bonds) will tend to spread over the second material. Liquids with strong cohesive bonds and weaker adhesive forces will tend to bead-up or form a droplet when in contact with the second material.

2.4 Capillarity

When a drop of liquid is placed on a solid surface, it will either spread across the surface to form a thin film or remain as a discrete drop on the surface, with some finite contact angle. The spreading of a very small, but macroscopic, drop is caused by capillarity, which is defined as the macroscopic motion of a fluid system under the influence of its own surface and interfacial forces [4].

In a capillary tube, or in a small drop of liquid, the surface tension forces create a pressure difference across the interface, and cause it to curve. The excess pressure across a curved interface is given by Laplace equation:

$$P_c = \gamma_{LV}(\frac{1}{R_1} + \frac{1}{R_2}) \qquad (2.1)$$

where γ_{LV} is the interfacial tension and R_1 and R_2 are the principal radii of curvature.

If the interface is a part of a sphere, then $R_1 = R_2$ ($=R$), and the equation becomes

$$P_c = \frac{2\gamma_{LV}}{R} \qquad (2.2)$$

The pressure across the curved surface of the drop (due to the liquid-vapour surface tension γ_{LV}), if not balanced by the solid surface tension (i. e. by $\gamma_{SL} + \gamma_{SV}$), causes the drop to spread. Such a spreading is similar to other types of hydraulic flow in that it results from the presence of a pressure difference between two hydraulically connected regions of the liquid mass. The direction of flow is such as to decrease the pressure difference. When the difference vanishes, or when there is no longer a mechanism to reduce the difference, flow (spreading) ceases [4]. The pressure differences arise as a result of differences in curvature of different regions of liquid fluid phase in the system and are due to the presence of an effective mechanical tension in the interface known as the surface or interfacial tension. The difference in curvature may result from different sources, including the application of external forces, the contacting and coalescence of two masses of the liquid

phase, or from the contact of the liquid phase with a second fluid phase and a solid surface [4].

2.5 Contact angle

The contact angle θ, shown in figure 2.2, "may be geometrically defined as the angle formed by the intersection of the two planes tangent to the liquid and solid surfaces at the perimeter of contact between the two phases and the third surrounding phase, which will be air or vapour" [4].
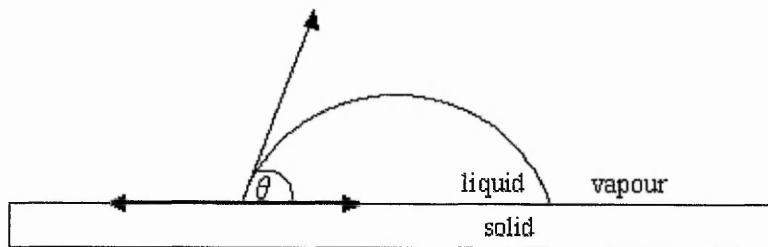
Figure 2.2. A schematic representation of the contact angle θ.

The contact angle measured using any optical method is called the apparent contact angle. The actual contact angle is the angle between the direction of the tangent to the solid surface at a given point and the direction of the tangent to the liquid-vapour interface at that point. This angle changes from one point to another along the contact line since most real solids are to some extent rough and chemically heterogeneous. The intrinsic contact angle is a unique property of a surface and defined by Young's equation (equation 1.1). Such an angle could be obtained on an ideal perfectly smooth, chemically homogeneous, rigid, insoluble and non- reactive solid surface [5].

2.5.1 Contact angle measurement techniques

Contact angles can be measured by using many methods. A description of two common methods, goniometery, tensiometery is given below. It should be noted that the goniometer gives the apparent contact angle while the tensiometer gives the actual contact angle.

2.5.1.1   Goniometery

A goniometer [6] basically consists of light source, sample stage, lens and image capture. This technique is based on analyzing the shape of the drop. The contact angle then is the angle formed between the solid and the tangent to the drop surface. The advantage of the Goniometer is that it needs a small quantity (a few microliters) of liquid for the measurement. The disadvantage is that it is subjective to the researcher in assignment of the tangent line. Consistency in measurements is achieved by introducing software (machine) analysis of the drop shape.

2.5.1.2   Tensiometry

A tensiometer [6] measures the forces on a solid sample in contact with a test liquid. The contact angle is then calculated when the force of interaction, the surface tension and the geometry of the solid is known. The Wilhelmy plate is an example of a tensiometer in which a thin plate is hung in a balance, and the reading (of the balance due to the plate weight) is adjusted to zero. The lower edge should be positioned in the same plane as the horizontal surface

of the liquid. The liquid is then raised to touch the plate. The imbalance that occurs on the contact is due to the weight of the entrained meniscus. Since the meniscus is held up by the tension on the liquid surface, the weight measured by the apparatus can be analysed to yield a value for the surface tension. The observed weight of the meniscus must equal the upward force provided by the surface according to the equation

$$w = p\gamma_{LV} \cos\theta \qquad\qquad (2.3)$$

where w is the weight (read by the balance), p is the plate perimeter, γ_{LV} is the liquid surface tension and θ is the contact angle. By suspending the plate from a sensitive balance, w can be measured with considerable accuracy. The perimeter of the plate can be measured, and if we use a liquid of known surface tension, then θ can be calculated from equation (2.3).

The advantages of this method is that it gives an average value of the contact angle of the entire perimeter of the solid, hysteresis can also be easily measured, and it can be used to measure the contact angles on fibers, which can't be measured using the goniometric approach. The disadvantages is that it needs enough liquid to immerse the solid in, and there are several requirements for the solid sample such as it must be formed in geometry that has a constant perimeter over a portion of its length, it must also have the same surface on each side that contacts the liquid and must be small enough to be hung to the balance of the tensiometer.

2.6   Wetting

The wetting ability of a liquid is a function of the surface energies of the solid-gas interface, the liquid-gas interface and the solid-liquid interface. The surface energy across an interface or the surface tension at the interface is a measure of the energy required to form a unit area of new surface at the interface. Understanding how wetting occurs needs knowledge of Young's equation and the spreading coefficient, which are described in the following sections.

2.6.1   Young's equation

Young's law (equation 1.1) can also be stated as,

$$\gamma_{LV} \cos\theta = \gamma_{SV} - \gamma_{SL} \tag{2.4}$$

where θ is the equilibrium contact angle, γ_{SV}, γ_{SL} and γ_{LV} are the solid-vapour, solid-liquid and liquid-vapour interfacial tensions respectively. Two types of proofs of equation (2.4) will be considered [3], the force proof and the energy proof.

i.   ***The force proof*** is illustrated in figure 2.3, which represents a sessile (sitting) drop. The solid-vapour surface tension tends to spread the drop that is to shift the three-phase line outwards (to the right). The solid-liquid interfacial tension and the horizontal component of the liquid-vapour surface tension ($\gamma_{LV} \cos\theta$) acts in opposite direction to the solid-vapour surface tension. In equilibrium, the net resultant force should be zero, hence Young's law (equation 2.4).
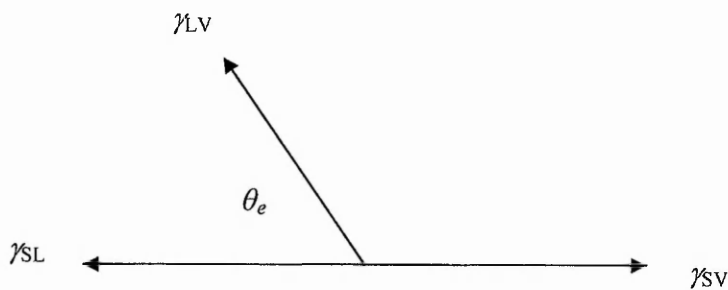
Figure 2.3. Interfacial forces on a sessile drop.

ii.   *The energy proof*
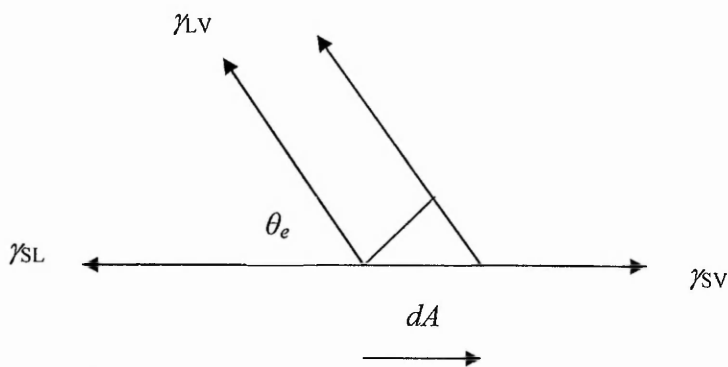
Figure 2.4. Minimum surface free energy approach to prove Young equation. The γ_{LV} in figure 2.3 is displaced by *dA*.

A system contains a liquid-vapour interface A_{LV}, a solid-vapour interface A_{SV} and liquid solid interface A_{SL}. If their extent changes, the free energy of the system is said to change by dF, (figure 2.4), then

$$dF = \gamma_{LV} dA_{LV} + \gamma_{SV} dA_{SV} + \gamma_{SL} dA_{SL} \qquad (2.5)$$

For a meniscus moving along a solid surface,

$$dA_{SV} = -dA_{SL} \qquad (2.6)$$

At the contact line a change dA_{SL} can be projected along the liquid-vapour interface as

$$dA_{LV} = \cos\theta \times dA_{SL} \qquad (2.7)$$

Introduction of equations (2.6 and 2.7) into equation (2.5) affords

$$dF = \gamma_{LV} \cos\theta \cdot dA_{SL} - \gamma_{SV} dA_{SL} + \gamma_{SL} dA_{SL} \qquad (2.8)$$

In equilibrium the change in the surface free energy dF equals zero for small

changes of dA_{SL}, thus Young's equation results.

2.6.2 The vertical component of liquid tension

In 1960 Bailey [7] conducted some experimental tests where she argued that

the vertical component of the Young's force is balanced by the strain field in

the solid. Shanahan and Carré [8] extended this argument to show that the

vertical component of the liquid vapour surface tension can lead to local

nanometric deformation of the soft substrate. Quéré deduced that the liquid-

vapour surface tension exerts all along the contact line a vertical force on the

solid, which resists because of its elasticity. The solid deformation (due to the

vertical forces) should be of the order of $\dfrac{\gamma_{LV}}{E}$, where E is a Young's modulus of

the solid [9]. The deformation is non-observable in hard solids, but it can

become appreciable in soft solids.

2.6.3 Spreading coefficient

Consider a surface of solid-vapour surface tension γ_{SV}. If the same surface is

covered by a thin liquid film, the surface tension is then the sum of the solid-

liquid surface tension γ_{SL} and the liquid-vapour surface tension γ_{LV}. The

spreading coefficient $S_{L/S}$ is defined as the difference in energy between the

two situations and is given by:

$$S_{L/S} = \gamma_{SV} - (\gamma_{SL} + \gamma_{LV}) \qquad (2.9)$$

Positive spreading coefficient means that γ_{SV} is greater than the sum $(\gamma_{SL} + \gamma_{LV})$, and therefore the system favours liquid spreading and is called in this case a high energy surface. Solid with strong intermolecular force (covalent, ionic or metallic) bonds are examples of high energy surfaces. Their typical surface free energy is between 500-5000 ergs/cm^2 [10]. On the other hand negative spreading coefficient means that γ_{SV} is less than the sum $(\gamma_{SL} + \gamma_{LV})$, and therefore the liquid favours forming a drop with a finite contact angle. Molecular solids which are usually bounded by van der Waals forces are examples of low energy surfaces with free energies around 50 ergs/cm^2 [10].

To encourage wetting, γ_{LV} and γ_{SL} should be made as small as possible. This can be done by adding a surfactant to the liquid phase to lower both the liquid-solid and liquid-vapour interfacial tensions [11].

2.7 Wetting hysteresis

Hysteresis is defined as the difference between the advancing and the receding contact angle. The advancing angle is obtained by adding liquid to the drop. Adding too much liquid causes drop spreading. The advancing angle just before this drop spreading occurs is the maximum advancing contact angle [3]. The receding angle is observed when a small volume of liquid is removed from the drop. When the drop becomes flat due to liquid withdrawal, it suddenly contracts, and the angle at which this happens is the minimum

receding angle [3]. The consequence of hysteresis is the existence of a range of contact angles on the same solid surface.

2.7.1 Causes of hysteresis

2.7.1.1 Chemical or physical heterogeneities of the surface

Chemical or physical heterogeneity of the surface is known to cause contact angle hysteresis [10-15]. Chemical heterogeneities involve surface contamination or deliberate chemical patterning of the surface by different chemical patches. Physical heterogeneities involve surface structuring and any other deliberate or accidental defect on the surface.

2.7.1.2 Volume change

Another cause of hysteresis suggested by some groups of researchers is volume change. Brenden *et al* [16] reported that the average contact angle hysteresis is found to exhibit a degree of volume dependence. Hysteresis was also reported during evaporation and condensation, which are processes accompanied by volume change [17,18]. See figure 2.5.
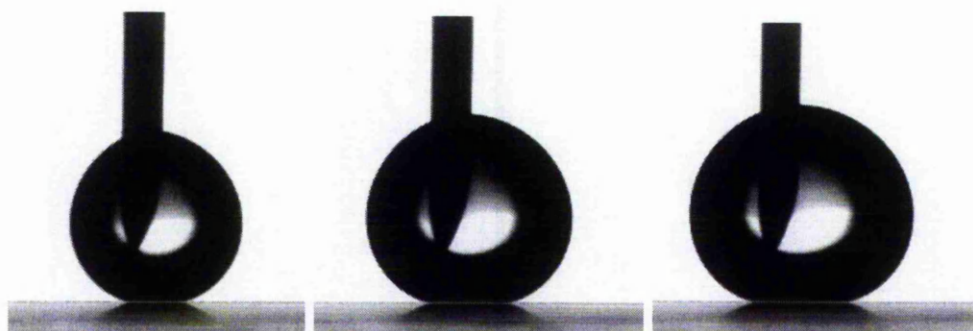
Figure 2.5 The drop volume increase from left to right resulting in decrease in the contact angle. Increasing the drop volume results in contact angle hysteresis. The contact angles are 153.6, 152.2, and 151.2 corresponding to volumes of 1.93, 2.44 and 2.90 microliters respectively. Note the change in the solid liquid area.

2.7.2 Methods of measuring hysteresis

2.7.2.1   Stage tilting method

The easiest way to measure hysteresis is to deposit a drop on the substrate and then tilt the stage on which the substrate is sitting (figure 2.6). The maximum advancing angle and the minimum receding angle are the angles photographed just before the drop moves (under the influence of gravity). Measurement of the contact angle hysteresis can be very tricky. Too small drops (for example) may not move even if the substrate is tilted vertically.
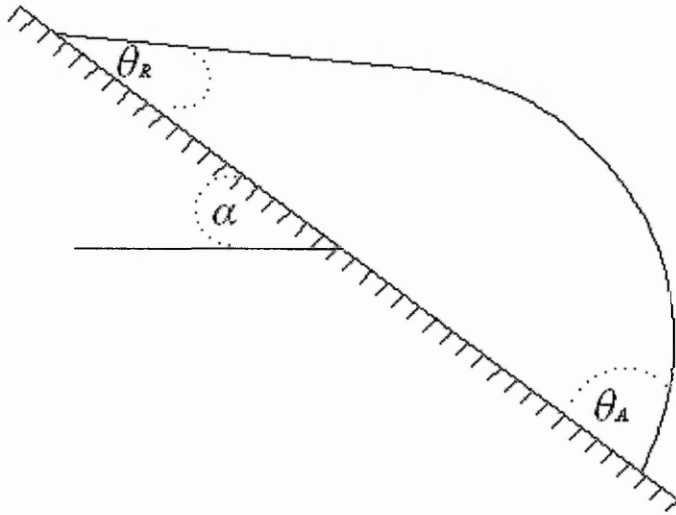
Figure 2.6. A drop on a tilted stage, θ_A is the advancing contact angle and θ_R is the receding contact angle, provided they are measured just prior to motion as the tilt angle α is increased.

2.7.2.2   Adding and withdrawing method

To measure the advancing angle, a small amount of liquid is added to the drop. The receding angle is measured whilst liquid is withdrawn from the drop [3]. Adding and removing liquid should be done without causing a sharp movement of the drop base i. e. with constant base radius (see figure 2.7).

(a)   **(b)**   **(c)**
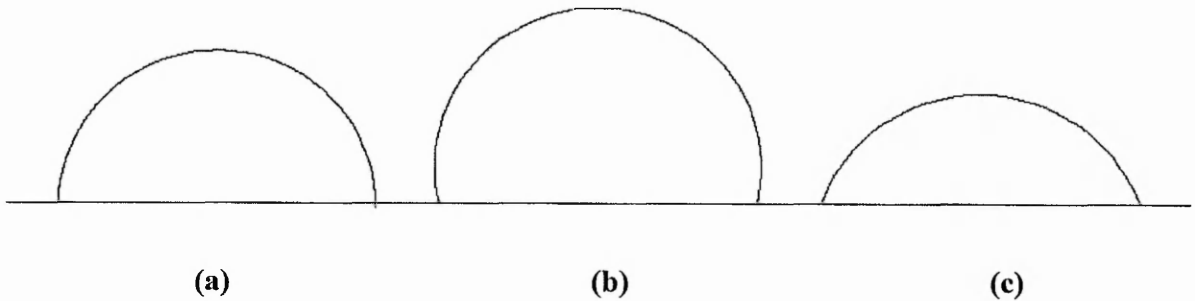
Figure 2.7. Contact angle hysteresis. The base of the drop does not change when volume increases from (a) to (b) or decrease from (a) to (c).

2.8   Models of contact angle on rough surfaces

2.8.1 Wenzel model

Wenzel's theory [12] of contact angle on a rough surface assumes that the liquid completely fills the troughs in the region of its contact with a rough substrate. The contact angle θ_e^W (on the rough surface) is then given by the Wenzel equation,

$$\cos\theta_e^W = r\cos\theta_e^S \tag{2.10}$$

where r is the roughness factor and is given by $r = A_{true}/A_{horizontal}$; θ_e^S is the equilibrium contact angle on the flat surface. To understand this consider the

patterned surface shown in figure 2.8. r is the solid surface roughness, and is defined as the ratio of the actual area of the solid-liquid contact to the projected area on the horizontal plane and in this particular example is equal to 1 plus the side area of the surface structure divided by the horizontal area. Displacing the liquid by dA results in a change in the surface free energy of dF, this is given by:

$$dF = -\gamma_{SV} r dA + \gamma_{SL} r dA + \gamma_{LV} dA \cos\theta \qquad (2.11)$$

At equilibrium $dF = 0$, so

$$0 = -\gamma_{SV} r dA + \gamma_{SL} r dA + \gamma_{LV} dA \cos\theta \qquad (2.12)$$

which gives

$$0 = dA\left(r(\gamma_{SL} - \gamma_{SV}) + \gamma_{LV} \cos\theta \right) \qquad (2.13)$$

And using Young law (equation 2.4) gives,

$$\cos\theta_e^W = \frac{r(\gamma_{SV} - \gamma_{SL})}{\gamma_{LV}} = r \cos\theta_e^S \qquad (2.14)$$
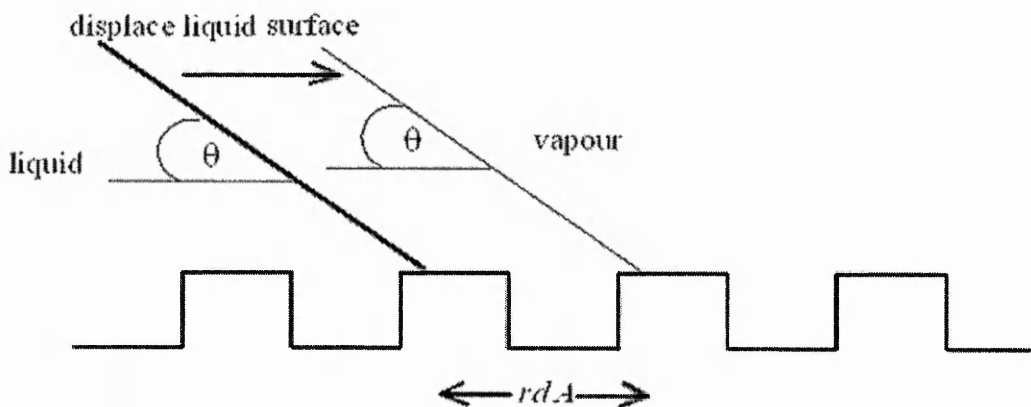
Figure 2.8. Wenzel model. Displacing the liquid-vapour interface results in change in the solid-liquid area by *rdA*.

2.8.2 Cassie-Baxter model

Cassie and Baxter assumed that the drop does not penetrate the troughs in the rough surface, but sits on the top of the rough surface with air underneath [13]. The contact angle is then an average between the value on air (that is 180˚) and on the solid (that is θ_e^s) and is given by

$$\cos\theta_e^{CB} = \phi_s \cos\theta_e^s - (1-\phi_s)$$ (2.15)

where ϕ_s is the solid fraction upon which the droplet rests.
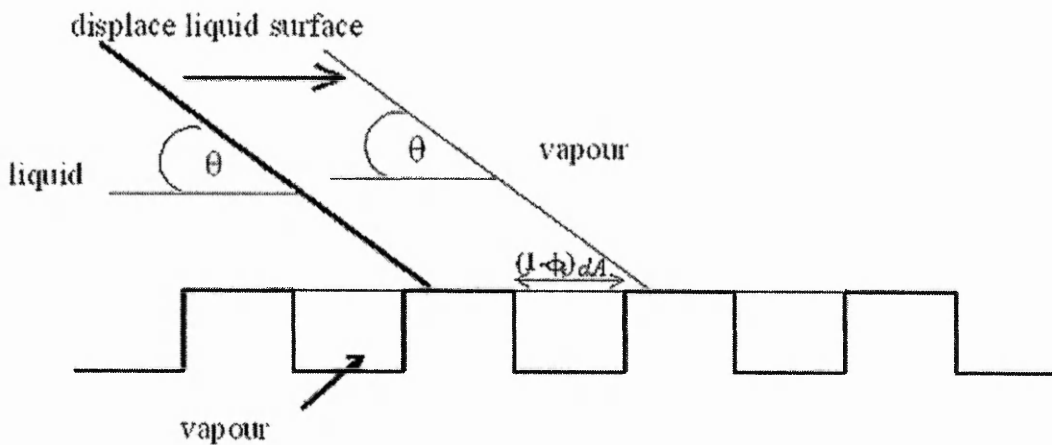
Figure 2.9. Cassie-Baxter model. Displacing the liquid-vapour interface results in change in the solid-liquid and liquid vapour area by ϕ_s dA and (1-ϕ_s) dA respectively.

Consider the patterned surface figure 2.9. ϕ_s is the solid surface fraction. Displacing the liquid by dA results in changing the surface free energy by dF, which is given by:

$$dF = \phi_S (\gamma_{SL} - \gamma_{SV})dA + (1-\phi_S)\gamma_{LV}dA + \gamma_{LV}dA\cos\theta$$ (2.16)

At equilibrium $dF = 0$, so

$$0 = dA(\phi_S(\gamma_{SL} - \gamma_{SV}) + \gamma_{LV}((1-\phi_S) + \cos\theta))$$ (2.17)

and using Young law (equation 2.4) gives,

$$\cos\theta_e^{CB} = \phi_s \cos\theta_e^s - (1-\phi_s)$$ (2.18)

2.9   Wenzel versus Cassie-Baxter angle: effect of pattern dimensions
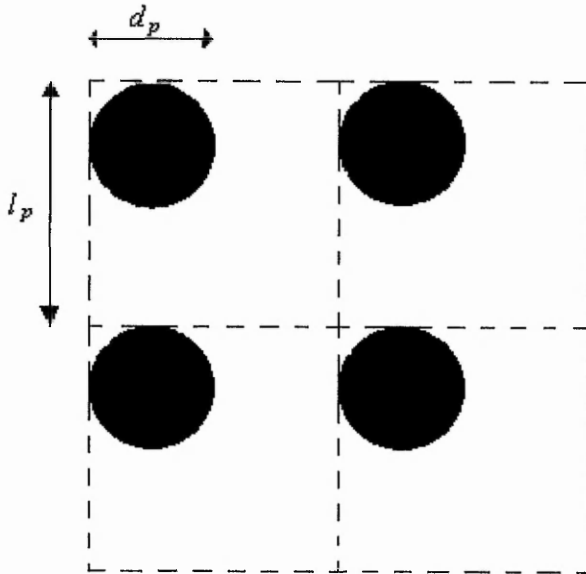
Figure (2.10). Schematic of the surface pattern.

Consider a surface structure that consists of circular cross sectional pillars of diameter d_p and height h_p arranged in a square lattice of period l_p as shown in figure (2.10).The roughness factor r is then given by,

$$r = 1 + \frac{\pi\, d_p\, h_p}{l_p^2}$$ (2.19)

and the solid fraction ϕ_s is,

$$\phi_s = \frac{\pi\, d_p^2}{4\, l_p^2}$$ (2.20)

When the pillar diameter is equal to the separation (i.e. $l_p=2d_p$), then $\phi_s=\pi/16=0.1963$. That means whatever the value of pillar diameter, the solid fraction remains constant [18]. On the other hand $r=1+\pi h_p/4d_p$, which implies that the roughness is a function of both the diameter and the pillar's height. Therefore the Cassie-Baxter angle in that case is constant while the Wenzel angle is a function of the pillars dimensions (height and diameter).

2.10 Rough hydrophobic surfaces

Roughening hydrophobic surfaces is proven to cause surface superhydrophobicity (a surface of contact angle greater than 150°). Two laws can be used to model such behaviour: Wenzel and Cassie-Baxter [19,20,21]. Each of the two models predicts quite different behaviour. In Wenzel the liquid penetrates the surface roughness and the resultant contact angle is deduced from the cosine of Young's angle multiplied by the roughness factor r (which is the ratio between the actual and the projected surface area). On the other hand, the Cassie-Baxter model involves air below the droplet, leading to a drop sitting on a composite surface made from the solid and air, and the contact angle is then an average between the contact angle on the solid and the contact angle in air (which is 180 degrees). Figures 2.11 and 2.12 show the predicted Wenzel and Cassie-Baxter angle for a rough hydrophobic surface.
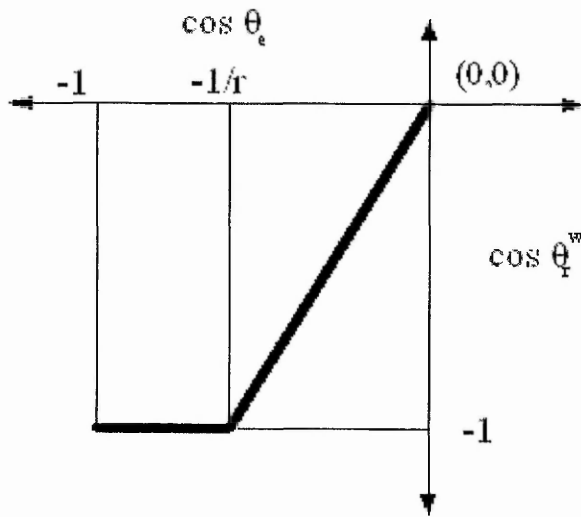
Figure (2.11). The predicted contact angle by the Wenzel equation [Ref. 20]
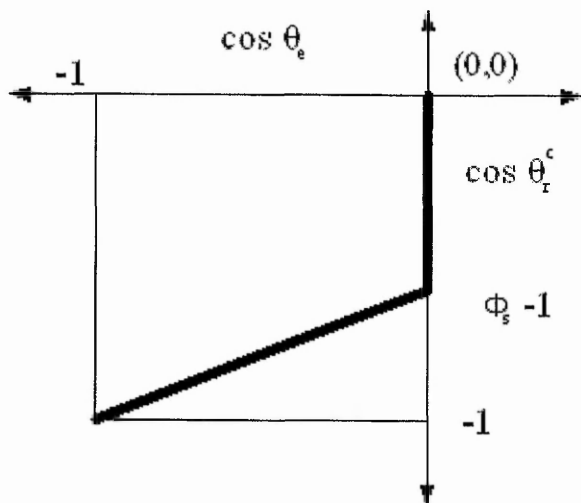
Figure (2.12). The predicted contact angle by Cassie-Baxter equation [Ref. 20]

The threshold between the two states occurs when [18,19]:

$$\cos\theta_{th} = (\phi_s - 1)/(r - \phi_s) \tag{2.21}$$

where θ_{th} is the angle where the two models meet for the same rough hydrophobic surface (figure 2.13).
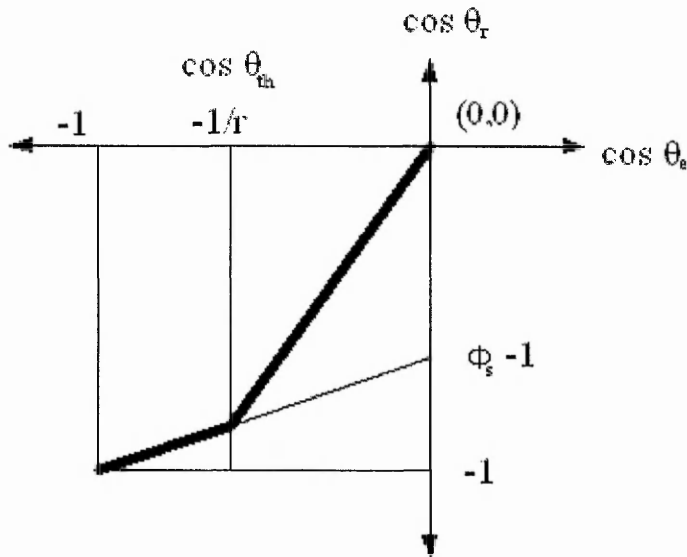
Figure 2.13. The threshold contact angle between the different models of superhydrophobicity. The Wenzel state should be selected for moderate hydrophobicity ($90<\theta_e<\theta_c$). For very hydrophobic material $\theta_e > \theta_c$ the Cassie model should be selected. [Ref. 17]

The Wenzel model implies that the liquid should follow the profile of the solid surface. If the surface is very hydrophobic, then following the surface profile is very costly in energy. This leads to a drop preferring the Cassie model. Also in the Cassie model the liquid-vapour area increases. This is unlikely to develop if the hydrophobicity is not high enough [19].

The main difference between the two models is the contact angle hysteresis [17,19,20,21]. While Wenzel suffers a great deal of hysteresis, Cassie-Baxter experiences a small degree of hysteresis. This is because Wenzel drop penetrates the surface structure and becomes pinned, while Cassie Drop remains suspended on the surface structure. The pinning of the contact line can be detected by tilting the substrate on which the drop rests. The Cassie

drop rolls at low tilt angles, while the Wenzel may not roll off even at high tilt angle. For a rough hydrophobic surface the Cassie model is preferred, however the Wenzel model can be induced by applying external force (for example applying pressure on the drop) or forming the drop through condensation and not deposition [17,19].

2.11 Wetting and the dynamics of spreading

The spreading of liquid drops on a smooth solid surface is caused mainly by interfacial tension effects, and is opposed by viscosity. In the following sections description of the different factors causing drop spreading are given.

2.11.1 Spreading driven by capillarity

Capillarity is defined as the macroscopic motion of a fluid system under the influence of its own surface and interfacial forces. For a droplet put on a solid surface the spreading is caused by the forces at the contact line arising from the three interfacial tensions γ_{SV}, γ_{SL} and γ_{LV} occurring at the solid-vapour, solid-liquid and liquid-vapour interfaces respectively.

Consider the forces affecting a drop on horizontal surface shown in figure 2.3. The forces along the x-axis are

$$F_x = \gamma_{SV} - \gamma_{SL} - \gamma_{LV} \cos\theta \qquad (2.22)$$

At equilibrium $\theta=\theta_e$ so F becomes the equilibrium force F_e, which is given by,

$$F_e = \gamma_{SV} - \gamma_{SL} - \gamma_{LV} \cos\theta_e \qquad (2.23)$$

The difference between the two situations is the net force F_{net}, which is given by,

$$F_{net} = F_x - F_e = \gamma_{LV}(\cos\theta_e - \cos\theta) \qquad (2.24)$$

If the drop is deposited with original contact angle different from the equilibrium one, it will spread until the contact angle is equal to the equilibrium contact angle. Complete wetting is achieved when the spreading factor (equation 2.9), is greater than or equal to zero, i.e. when the solid-vapour

surface tension γ_{SV} is greater than or equal to the sum of the liquid-solid γ_{SL}

and liquid-vapour γ_{LV} interfacial tensions.

2.11.2 Spreading driven by the Marangoni effect

Marangoni driven spreading occurs when there is a surface tension gradient. Temperature and surfactant concentration gradient along the drop surface causes surface tension gradient, which results in tangential stress at the surface, giving rise to fluid motion in the underlying bulk liquid [22]. The tangential force per unit area is given by

$$F = \nabla \gamma \qquad (2.25)$$

where $\nabla \gamma$ is the surface tension gradient. Positive $\nabla \gamma$ indicates that the liquid tends to move in a direction from low to high surface tension. The liquid droplets move spontaneously over the solid surface without the application of external force.

2.11.3 Other factors affecting spreading

The other forces that affect the spreading include:

1) Gravity. It can be neglected for drops of sizes less than the capillary length of the liquid κ, which is defined as

$$\kappa = \sqrt{\frac{\gamma_{LV}}{\rho g}} \qquad (2.26)$$

where γ_{LV} , ρ and g are the liquid surface tension, density and the acceleration due to gravity, respectively.

2) Intermolecular forces [10,23]. The long range (van der Waals) forces affect drop spreading. The role of the van der Waals forces is pronounced in very small drops and can be neglected for macroscopic scales. They are attractive or repulsive forces, depending on situation, and generally do not adhere to single power law with respect to their dependence on separation distance. Their effect in some cases extends to a range of 10 nm or more [4].

3) Surface roughness. Surface roughness modifies the net balance of forces [24,25]. See also section 2.11.5.

2.11.4 Drop spreading on a smooth surface

In this section, the spontaneous spreading of drops that wet completely horizontal solid surface is discussed. To simplify the problem of drop spontaneous spreading, one has to work with very small (compared to the capillary length) viscous drops, where gravity can be neglected.

In 1975 Hoffman studied the system described above by measuring the apparent contact angle (by photographic techniques) and found that in the low velocity limit, the drop edge velocity is proportional to the dynamic contact angle according to the relation [26].

i.e $v_E \propto \theta^p$ (2.27)

where θ is the dynamic contact angle, and with $p=3$.

The magnitude of the spreading parameter $S_{L/S}$ (equation 2.9) has no influence on the drop edge velocity [10].

The same system was also chosen by Tanner (1979) who followed the spreading of a number of viscous silicone oils on smooth horizontal surfaces [27]. In his low velocity experiments, Tanner assumed that, for a liquid that spreads completely on a surface, the dynamics of the wetting is controlled by the hydrodynamic regime, i.e. only capillarity and viscous forces. By equating the viscous dissipation to the rate of work done by the capillary forces, he showed that the drop edge speed is proportional to the cube of the contact angle (equation 2.27) and the dynamic contact angle is a power law in time (equation 2.28)

$$\theta \propto t^{-n} \tag{2.28}$$

with $n=0.3$ for drops spreading on a horizontal flat surface.

The drop base diameter-time relation was also given by Tanner as

$$d \propto t^{-m} \tag{2.29}$$

with $m=0.1$.

The mathematical justification of equation 2.27 given below follows reference [24]:

When a drop spreads on a flat surface, a Poiseuille flow occurs and a viscous dissipation proportional to $\dfrac{\eta v_E^2}{\theta}$ is created, where η is the viscosity, v_E is the

edge speed of the drop. This dissipation is proportional to unbalanced component of the liquid vapour surface tension $\gamma_{LV}\left(\cos\theta_e^s - \cos\theta\right)$, i. e.

$$\frac{\eta v_E^2}{\theta} \propto \gamma_{LV}\left(\cos\theta_e^s - \cos\theta\right)v_E \qquad (2.30)$$

When θ_e^s is equal to zero, the equation becomes

$$\frac{\eta v_E}{\theta} \propto \gamma_{LV}\left(1 - \cos\theta\right) \qquad (2.31)$$

For small angles $\left(1-\cos\theta\right) = (1-1+\dfrac{\theta^2}{2}-...)$ $\qquad (2.32)$

This means $\dfrac{\eta v_E}{\theta} \propto \gamma_{LV}\theta^2$ $\qquad (2.33)$

i. e. $v_E \propto \dfrac{\gamma_{LV}}{2}\theta^3$ $\qquad (2.34)$

which is Hoffman's law for spreading on flat surfaces: the drop edge speed is proportional to the cube of the contact angle.

2.11.5 Drop spreading on rough surfaces

For a drop spreading on a rough surface [24] the dissipation is again proportional to unbalanced component. However the roughness factor must now appear in the unbalanced force so that when the force vanishes, Wenzel equation is obtained. Equation 2.31 is then modified to

$$\frac{\eta v_E^2}{\theta} \propto \gamma_{LV}\left(r\cos\theta_e - \cos\theta\right)v_E \qquad (2.35)$$

so that when $\theta_e^s = 0$, the equation becomes,

$$\frac{\eta v_E}{\theta} \propto \gamma_{LV}(r - \cos\theta) \tag{2.36}$$

$(r - \cos\theta)$ can be expanded to give

$$(r - \cos\theta) = (r - 1 + \frac{\theta^2}{2} - ...) \tag{2.37}$$

and equation (2.36) becomes

$$\frac{\eta v_E}{\theta} \propto \gamma_{LV}\left(r - 1 + \frac{\theta^2}{2} - .....\right) \tag{2.38}$$

For small angles the series can be approximated to:

$$\frac{\eta v_E}{\theta} \propto \gamma_{LV}(r - 1) + \frac{\gamma_{LV}}{2}\theta^2 \tag{2.39}$$

which gives

$$v_E \propto \frac{\gamma_{LV}}{\eta}(r - 1)\theta + \frac{\gamma_{LV}}{2\eta}\theta^3 \tag{2.40}$$

For small contact angles the second term is negligible thus leading to a modified Hoffmann Law

$$v_E \propto \frac{\gamma_{LV}}{2\eta}\theta \tag{2.41}$$

Thus, for smooth surfaces a cubic law is obtained and this tends to a linear law as roughness is introduced.

The modification of the dynamic contact angle-time relation due to surface roughness was shown to follow the power law (equation 2.28), but with the exponent n changing from $n=3/10$ to $n=3/4$ [24].

i. e $\theta \propto t^{-\frac{3}{4}}$ \hfill (2.42)

and the base diameter-time relation becomes

$$d \propto t^{0.25} \qquad\qquad\qquad\qquad\qquad (2.43)$$

These predicted relations for drops spontaneous spreading on rough surfaces will be investigated experimentally and presented in chapter 4.

2.12 Wetting and evaporation

Evaporation of a droplet on both smooth and rough surfaces can cause changes in both contact angle and contact diameter. For evaporation from non-superhydrophobic surfaces several attempts have been made to calculate the diffusion constant. Of particular interest is the special case of the constant contact radius mode. These models all assume that the rate of change of mass of an evaporating drop can be calculated on the basis of the diffusion of water molecules from the droplet surface into the surrounding atmosphere. For completely spherical droplet, the rate of mass loss of liquid is given by

$$\rho_L \frac{dV_C}{dt} = -4\pi R_S D \Delta c \tag{2.44}$$

where ρ_L is the liquid density, R_S is the spherical radius, V_C is the volume, D is the diffusion coefficient of water vapour into the surrounding air, and $\Delta c = (c_S - c_\infty)$ is the concentration difference, which is the difference between the vapour concentration at the droplet surface (assumed to be equal to the saturation concentration c_S) and ambient value far removed from the droplet surface (c_∞).

Picknett and Bexon [29] predict that for a completely spherical droplet in contact with a substrate (i.e. a contact angle up to 180°), the evaporation will reduce due to the reduction in space into which vapour can diffuse. Therefore equation (2.44) is modified by a factor of $f_{PB}(\theta)$, so the equation becomes

$$\rho_L \frac{dV_C}{dt} = -4\pi R_S D\Delta c f_{PB}(\theta) \tag{2.45}$$

where $f(\theta)$ is a function of the contact angle θ. Picknett and Bexon gave two empirical polynomial fits to $f(\theta)$ covering the angular ranges, 0-10 and 10-180°,

$$2f_{PB}(\theta) = \begin{cases} 0.6366\theta + 0.09591\theta^2 - 0.06144\theta^3 & 0° < \theta < 10° \\ 0.00008957 + 0.6333\theta + 0.116\theta^2 - 0.08878\theta^3 + 0.01033\theta^4 & 10° < \theta < 180° \end{cases} \tag{2.46}$$

where θ is in radian.

The following section provides a theoretical method for calculating $f(\theta)$, in the constant contact radius mode, which can be used in equation (2.45) for a drop on a superhydrophobic surface to find the value of the diffusion constant-vapour concentration difference product ($D\Delta c$) in the constant contact radius mode. The mathematical justification follows reference [19].

2.12.1 Constant contact radius mode

The volume of a spherical cap drop is given by,

$$V_C(r_b, \theta) = \frac{\pi r_b^3 (1 - \cos\theta)^2 (2 + \cos\theta)}{3\sin^3\theta} \tag{2.47}$$

where r_b is the contact (or base) radius of the droplet. In the contact radius mode, the rate of change of volume can be written in terms of the rate of change of the cosine of the contact angle [30],

$$\frac{dV_C}{dt} = \frac{-\pi r_b^3}{(1-u^2)^{1/2} (1+u)^2} \left(\frac{du}{dt}\right) \tag{2.48}$$

where $u=\cos\theta$. Since, $r_b=R_S\sin\theta$ and $\sin\theta=(1-u^2)^{1/2}$, where R_S is the spherical radius, substituting equation (2.48) into equation (2.45) gives,

$$\frac{u^n}{2 f_{PB}(\theta)(1+u)^2} \left(\frac{du}{dt}\right) = \frac{2D\Delta c}{\rho_L\, r_b^2} \tag{2.49}$$

where $n=0$

which cannot be integrated exactly in its present form. However, terms of the form $u^n/(1+u)^2$ are integrable and so a polynomial can be developed to fit to $2f_{PB}(\theta)$, accurate to 0.04% at all angles, for our range of interest of 90° to 180°,

$$\frac{1}{2 f_{PB}(\theta)} \approx \sum_{n=0}^{3} d_n u^n = 0.999766 + 0.481517u + 0.292040u^2 + 0.089118u^3 \tag{2.50}$$

Substituting equation (2.50) into equation (2.49) and integrating gives,

$$H_{PB}(\theta) \equiv \frac{-e_0}{1+u} + e_1 \log_e(1+u) + e_2 u + e_3 u^2 = \frac{-2D\Delta ct}{\rho_L r_b^2} + H_{PB}(\theta_o) \tag{2.51}$$

where $u(t)=\cos\theta(t)$ and the constants e_n are given by,

$$\begin{aligned}
e_o &= d_0 - d_1 + d_2 - d_3 &&= 0.721171 \\
e_1 &= d_1 - 2d_2 + 3d_3 &&= 0.164791 \\
e_2 &= d_2 - 2d_3 &&= 0.113804 \\
e_3 &= d_3/2 &&= 0.044559
\end{aligned} \tag{2.52}$$

and are valid over the contact angle range 90° to 180°. The constant $H_{PB}(\theta_o)$ is a constant of integration and represents the function evaluated at the contact angle for the initial time $t=0$.

Equation (2.51) can be used to calculate the product $D\Delta c$ in pinned contact radii mode for drops evaporating with initial contact angles greater than 90°. By plotting the function $H_{PB}(\theta)$ against time, t, the data for any given droplet should lie on a straight line and the slope, multiplied by $-\rho_L\, r_b^2/2$, will provide an estimate of the diffusion constant-vapour concentration difference product (i.e. $D\Delta c$). ρ_L is the liquid

In a similar way, the diffusion constant-vapour concentration difference product ($D\Delta c$) can be obtained from the rate of area change. Assuming a spherical droplet, the surface area of the liquid-vapour interface is given by,

$$A_{LV} = \frac{2\pi r_b^2}{1+\cos\theta} \tag{2.53}$$

Differentiating equation (2.53) gives

$$\frac{dA_{LV}}{dt} = -\frac{2\pi\, r_b^2}{(1+u)^2}\left(\frac{du}{dt}\right) = -\frac{u^0}{(1+u)^2}\left(\frac{du}{dt}\right)2\pi r_b^2 \tag{2.54}$$

Equation (2.49) can be rearranged into

$$\frac{u''}{(1+u)^2}\left(\frac{du}{dt}\right) = \frac{4f(\theta)D\Delta c}{\rho_L\, r_b^2} \tag{2.55}$$

Substituting equation (2.54) into equation (2.55) results

$$\frac{dA_{lv}}{dt} = \frac{-8\pi D\Delta c f\theta}{\rho_L},$$
(2.56)

where $f(\theta)$, is calculated from equation (2.50).

Equation (2.56) can be also be used to calculate the product $D\Delta c$ in pinned contact radii mode.

Chapter 5 will include values of the diffusion constant-vapour concentration difference product (i.e. $D\Delta c$) calculated from equation (2.51) and (2.56).

References

1. P. C. Hiemenz, R. Rajagopalan, Principles of Colloid and Surface Chemistry, 3rd revision, *New York: Marcel Dekker,* **1997**.

2. D. R. Lide, CRC Handbook of Chemistry and Physics, *CRC Press*, 81st Edition, **2000-2001**, 6-155.

3. J. J. Bikerman, Physical Surfaces, *Academic press*, **1970**.

4. D. Myers, *VCH Publisher, Inc.*, Surfaces, Interfaces and Colloids, **1991**.

5. A. Marmur, *Colloids and Surfaces A: Physicochemical Engineering Aspects*, 116, **1996**, 55.

6. www.ksvinc.com (accessed July 2005)

7. A. I. Bailey, *Proceeding 3rd International Conference*, Surface Activity Cologne, **1960**.

8. Shanahan M. E. R., Carre A, *Colloids and Surfaces A: Physiochemical and Engineering Aspects*, 206, 1, **2002**, 115.

9. D. Quere, *Physica A*, 313, **2002**, 32

10. P. G. De Gennes, *Review of Modern Physics,* 57, **1985**, 827.

11. A. W. Adamson A. P. Gast, physical chemistry of surfaces, sixth edition, *Wiley*, **1997**.

12. R. N. Wenzel, *Industrial Engineering Chemistry*, 28, **1936**, 988.

13. A. B. D. Cassie, S. Baxter, *Transaction of Faraday Society*, 40, **1944**, 546.

14. R. E. Johnson, R. H. Dettre, *Advances in Chemistry Series*, 43, **1964**, 12.

15. E. Rulon, J. R. Johnson, R. H. Dettre, *The Journal of Physical Chemistry*, **1964**, 1744.

16. S. Brendan, N. Haimovich, E. Yeger, A. Murmur, *Journal of Colloid and Interface Science*, 263, **2003**, 237.

17. A. Lafuma, D. Quere, *Nature letters,* **2003**, 457.

18. G. McHale, S. Aqil, N. J. Shirtcliffe, M. I. Newton, H. Y. Erbil, *Langmuir,* 21, **2005**, 11053.

19. D. Quere, A. Lafua, J. Bico, *Nanotechnology*, 14, **2003**, 1109.

20. N. Patankar, Langmuir, 19, **2003**, 1249.

21. B. He, N. A. Patanker, J. Lee, *Langmuir*, 19, **2003**, 4999.

22. A. D. Nikolov, D T. Wasan, A. Chengara, K. Koczo, G. A. Policello, I. Kolossvary, *Advances in Colloid and Interface Science*, 96, **2002**, 325.

23. L. M. Hocking, *Physics of fluids,* 6, 10, **1994**, 3224.

24. G. McHale, M. I Newton, *Colloid and Surfaces A*, 206, **2002**, 193.

25. G. McHale, N. Shirtcliffe, S. Aqil, C. C. Perry, M. I. Newton, *Physical Review Letters*, **2004**, 93.

26. R. L. Hoffman, *Journal of Colloid and Interface Science*, 50, **1975**, 228.

27. L. H. Tanner, *Journal of Physics, Applied Physics*, 12, **1979**, 1473.

28. G. McHale, S. M Rowan, M. I. Newton, *Journal of Physics, Division of Applied Physics*, 27, **1994**, 2619.

29. R. G. Picknett, R. J Bexon, *Journal of Colloid and Interface Science*, 61, **1997**, 336.

30. C. Bourgès-Monnier, M. E. R Shanahan, *Langmuir*, 11, **1995**, 2820.

Chapter 3

Experiments

3.1 Introduction

This chapter describes the experimental techniques used in this work.

The idea of this work was to study the effect of surface topography on its wetting property. To manipulate surface topography a photolithographic technique was used. The technique is explained in details in the beginning of this chapter. After that another technique for changing surface topography (electrodeposition) is described. However the attention is focused on the photolithography, because the thesis is about the wetting of microstructured surfaces.

Varieties of equipment and method can be used to characterize surface topography. The equipments used here are the scanning electron microscopy (SEM) and the confocal microscopy, which are described in this chapter. The contact angle measurement was also used as a method of surface characterization. This is described as well. The experimental arrangement and equipment used in contact angle measurement and in studying the spreading of PDMS oil droplets and the evaporation of water droplets from patterned surfaces are described.

3.2 Photolithography

Microstructured patterned surfaces were fabricated using a photolithographic technique, which was developed into a reliable technique for the production of large areas of high aspect ratio patterns [1]. Photolithography is defined as the process of transferring geometric shapes on a mask to a surface coated with a photosensitive polymer (a photoresist) [2]. When developed those regions of photoresist exposed to a given wavelength of light harden, while the unexposed dissolve in the developer leaving a pattern behind (this is for a negative photoresist).

The photoresist used in this study is the negative photoresist SU-8 50 from Microposit. It is epoxy based and becomes strong, stiff and chemically resistant after processing. It can be diluted using its developer PGMEA (1-methoxy 2-propyl acetate) from Aldrich to produce thinner layers and this offers a means to control the height of surface features. After exposure to radiation of specific wavelength (350-400nm) and postbaking, the resist becomes chemically inert, yielding a clean lift-off, which is extremely difficult to remove [3]. For this reason it can be left in devices like wave guides [4, 5].

Much of the work done previously using SU-8 has involved relatively large-scale patterns, (>50μm) but finer patterns with high aspect ratio have also been produced [6]. The SU8 homepage provides detailed information about its physical and chemical properties [7].

In this thesis work pillars of SU-8 50 were fabricated on glass cover slips coated with a film of the photoresist SU-8 50. This layer was spun, prebaked, exposed to ultraviolet and post baked to harden it. The reason of doing this was to ensure the same chemical homogeneity of the pillars and the area in between, and to improve the pillars' adhesion. Details about the influence of processing conditions such as baking temperature and UV dosage, on the thermal and mechanical properties of SU-8 coating (leading to better adhesion and avoiding coating shrinkage) can be found in ref. [8]. Height control of the pillars was achieved by varying either the concentration of the SU-8 50 or the speed of the spin coater or both.

In the following section a description of the experimental procedures developed to produce a patterned surface is given.

3.2.1 Stages of photolithography

Cleaning

The first step of lithography is surface cleaning. The cover slips were cleaned thoroughly because any dirt reduces the pattern adhesion. This was done in 3 stages: a substrate was first immersed into a solution of 2% Decon 90 (98% water), and sonicated in an ultrasound bath to remove any dust particles attached to it. Secondly it was rinsed with deionized water and finally rinsed with ethanol before drying using a stream of unfiltered nitrogen gas.

Water elimination

Surfaces were heated at 180°C for 5 minutes to remove any water. Cleaning and water elimination is crucial for obtaining a pattern that adheres properly to the surface.

Spinning

The aim of this stage is to produce a uniform layer of the photoresist of a given thickness. A layer of SU-8 50 was spread out using a glass pipette. Samples were then covered and left to stand for 15 minutes to allow bubbles in the SU-8 50 to escape. Spinning was carried out on an electronic Microsystems 4000 spin coater in a fume cupboard. Samples were spun in two stages: first at 500 revolution per minute (rpm) for 10 seconds to level the photoresist and then for some value between 2000 and 5000 rpm for 30 to 60 seconds, depending on the desired thickness. Figure 3-1 shows the relation between spin speed and layer thickness of the undiluted (100%) SU-8 50. It should be noted that the

SU8-50 layer was first spun at 500 rpm for 10 seconds before increasing the speed to the value shown in the figure. The exposure time here was kept constant (140s).
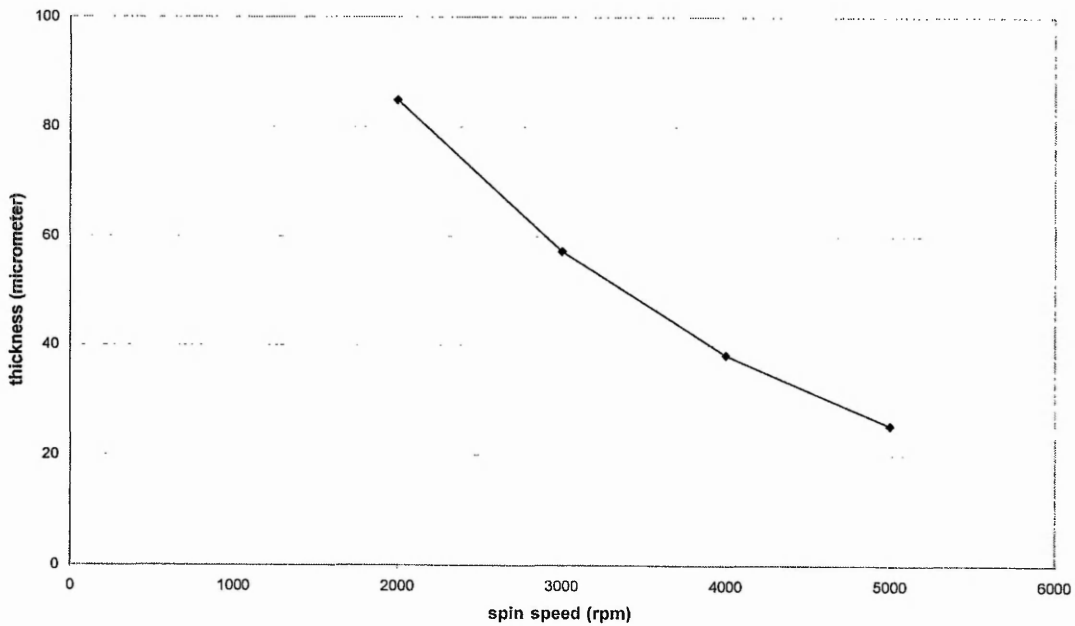
Figure 3.1. Film thickness versus spin coater speed for the undiluted photoresist SU8-50.

Pre-baking

Prebaking is the step in which the solvent is removed. The samples coated with the photoresist layer were pre-baked on a hot plate (which needed to be flat) for one minute at 65° C followed by 20 minutes at 95° C. Lower initial bake temperature allows the solvent to evaporate at more controlled rate, which results in better coating and improve the adhesion [9]. Over pre-baking degrades the photosensitivity of the photoresist.

Ultra-violet exposure

The soft baked photo-resist was exposed to the ultraviolet (UV) light through a mask. The mask aligner used is Cobalt C-800 mask aligner. The mask composes transparent circular areas separated by dark areas (figure 3.2). The areas under the transparent part of the mask become hard, while those under the dark areas remain soft, and then dissolve in the developer. SU-8 50 is virtually transparent and insensitive above 400 nm, but has high actinic UV-absorption below 350 nm [9]. Therefore excessive dose below 350 nm results in T topping profile (wide tops and thin bottoms). The optimal exposure dose depends on film thickness [9]. Under exposure causes pillar weakness, and results in them falling over during the developing stage; see figure (4.1) in the result and discussion chapter.
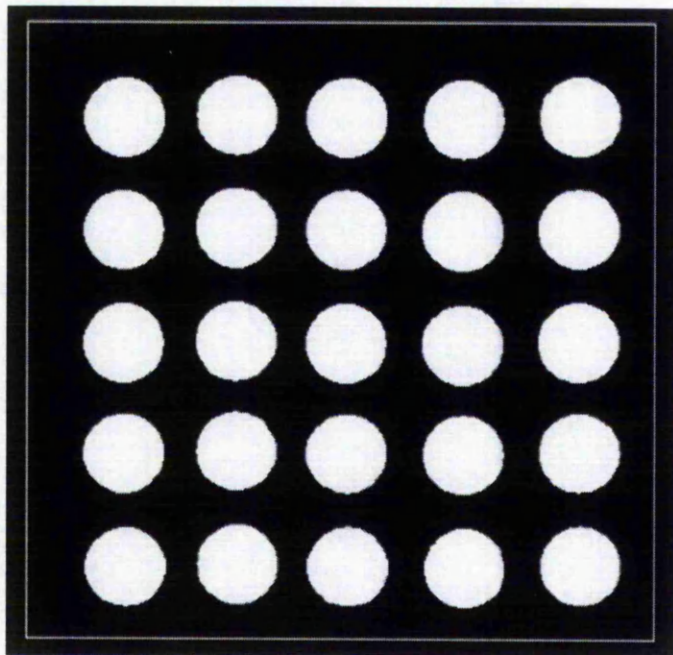
Figure 3.2. Mask consisting of circular transparent areas arranged in a square lattice.

Post-baking

The aim of this stage is to harden the photoresist and improve the adhesion to the surface, so the pillars don't fall over during the development. The post-baking was gradual. The temperature of the hot plate was increased from room temperature to 55°C and held for 10 minutes, it was then increased to 70°C and held for a further 10 minutes, then it was raised to 90°C for 10 minutes, and finally to 110 °C for 20 minutes. After the final heating stage the hot plate was switched off and it was allowed to cool undisturbed for approximately 2 hours. This slow cooling was found to improve the adhesion of the photoresist to the substrate [1].

Developing

After post baking the surfaces were developed in SU-8 50 developer and then rinsed using isopropanol and left in diethyl ether for 1 minute. The areas that were not exposed to UV dissolve in the developer, while the exposed areas remain hard.

3.3 Copper electrodeposition

"Electrodeposition of Copper onto flat copper electrodes produced randomly rough surfaces" [10]. Within this regime growth of deposits occurs in a dendritic, fractal manner. It should be noted that some research groups produced periodic structures from electrodeposition by periodic variation of cell voltage at -4°C and cell current of 30 µA [11].

The electrolytic cell shown in figure 3.3 is a schematic representation of the electro-deposition process
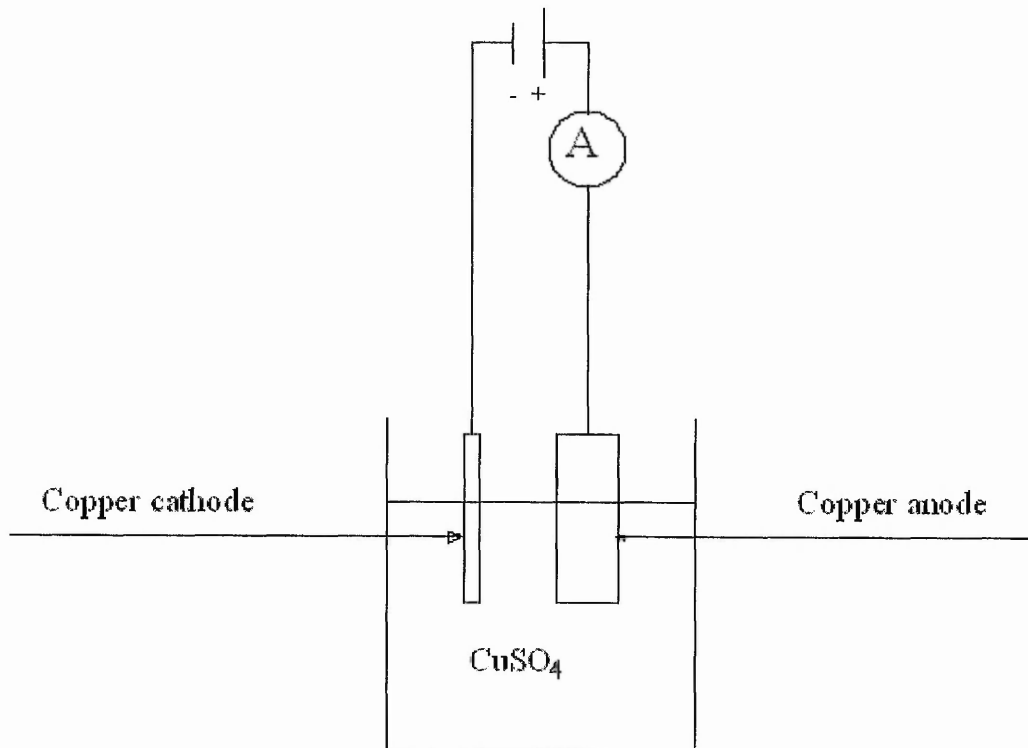
Figure 3.3. Electrodeposition cell

The cathode is a copper plate coated with nail polish except for a square of 1x1cm in the centre of the plate, which defines the area where the copper ions are deposited. The anode is another copper plate that has area of at least four times the cathode. The two plates were immersed in an acidified (few drops of H_2SO_4 are added to create acidic copper bath) copper sulphate solution of concentration of 200g/L. The power supply was then turned on and the voltage increased until the ammeter reads 200 mA and this was maintained for 2 minutes before turning the voltage down to zero. The copper sulphate dissociates in water to positively charged copper cations and negatively

charged sulphate anions. When the power is switched on the negatively charged copper plate (the cathode) attracts the positively charged copper cations, where the electrons flow from the negative electrode to the cations to neutralized them (or to reduce them) to metallic form. Meanwhile the negatively charged sulphate anions are attracted to the positively charged copper plate (the anode). At the anode electrons are removed from the copper metal, oxidizing it to the copper cations. The surface roughness is increased by increasing the current intensity [10].

3.4 Chemical treatment of rough surface

Two hydrophobizing agents were used in this study. The first is called Flutec (supplied by F_2 CHEMICALS LTD). It was used to hydrophobize the patterned surfaces. To ensure an even coating of the patterned surface, Flutec was dropped using a glass pipette onto samples when they were spun on the spin coating instrument. The second hydrophobizing agent used was Grangers Extreme Wash In, which is a commercial hydrophobizing agent. It was used for hydrophobizing rough surfaces prepared using electrodeposition. Grangers was diluted in deionized water by a factor of 50. The samples were then immersed in the solution at room temperature for 20 minutes before drying with a nitrogen gas stream. After that they were left in a drying oven for 20 hours at 40°C.

3.5   Surface characterization

3.5.1 Scanning electron microscope

Specifications

The scanning electron microscope (SEM) used was a JSM-840A. At 39 mm working distance and at 35kV power, the resolution is 10 nm and the magnification range is 10-300,000. The sample can be tilted up to 78° [11]. This is needed to obtain a view of the pillar sides. In this study the working distance was 39 mm, and the voltage used was between 3 and 6 kV. In most of the samples this gave a good sharp image of the pillars.

Sample preparation:

Because a SEM illuminates the sample with electrons, the sample has to be conductive. The SU-8 50 surfaces were made conductive by coating them with a very thin layer (few hundreds of nanometer) of gold using a sputter coater. The samples were viewed from the top to measure pillar diameter and separation, and then were tilted to some angle in order to view and measure the height of the pillars (taking into account the known tilt angle).

3.5.2 Confocal microscope

Specification

The confocal microscope used in this study was a Leica TCS NT. It was used to view some of the samples (especially those whose separation was nominally equal to the diameter). It gave clear information about the diameter-separation

ratio and because, unlike with the SEM, the sample doesn't need any coating it was also used in the spreading experiments for viewing the ingress of films of oil into patterned surfaces.

3.6 Contact angle measurement

A Krüss DSA10 contact angle meter (video profilometry with drop shape analysis software) was used to determine the contact angle (i.e, the tangent angle at the contact line between the liquid and vapour measured from the solid-liquid interface) from a side view of the drop. The side view profile of the drop could provide apparently good symmetry approximate to a spherical cap [13]. In some experiments a microscope was used to obtain a top view of the drop and visually asses whether the drop possessed axial symmetry.
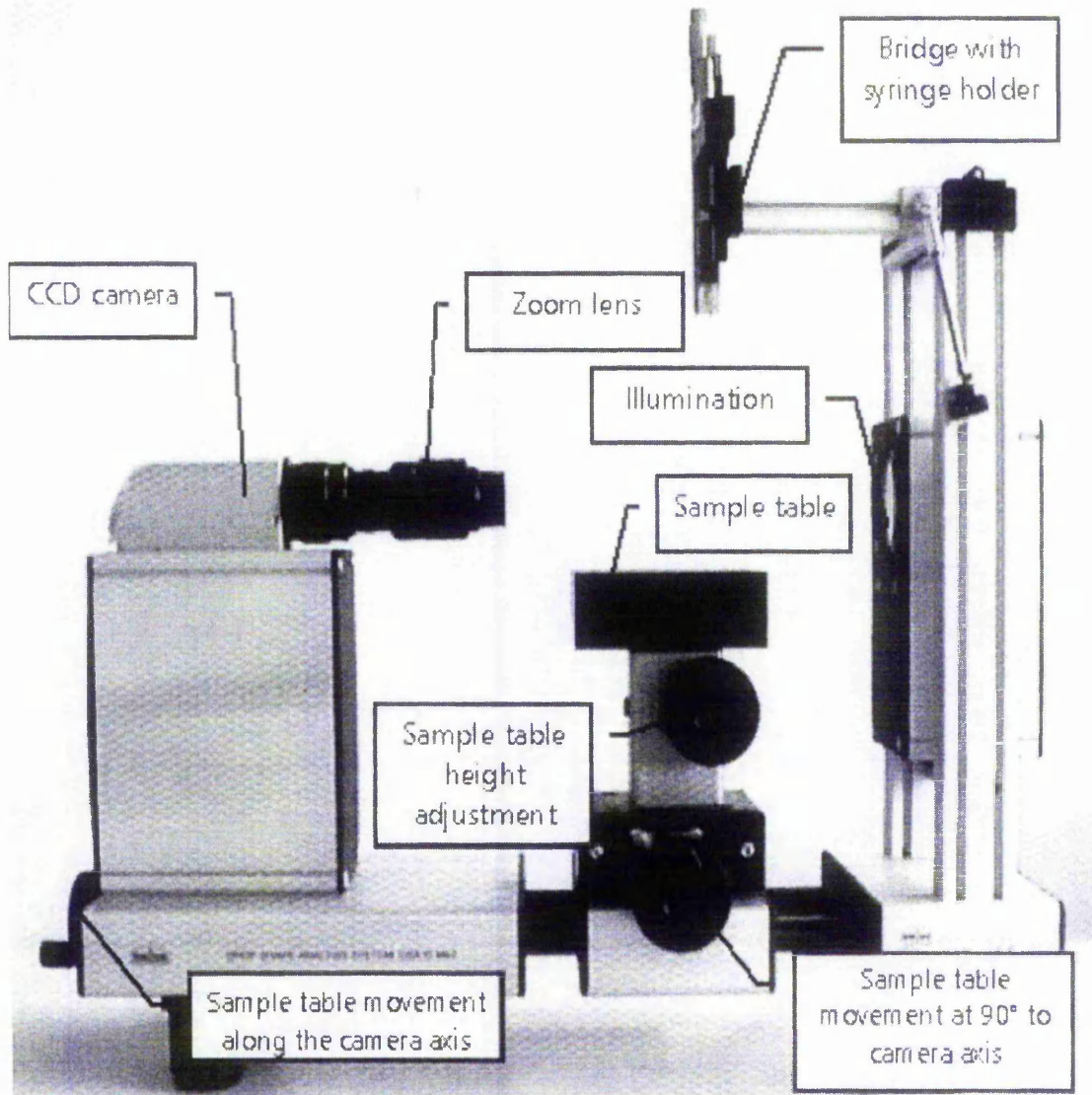
Figure 3.4 shows the components of the Krüss system.

Figure 3.4. Krüss system components.

- The CCD Camera is attached to video controlled by the Krüss software, which can be programmed to acquire a certain number of frames per second.

- The volume of the drop, dispensed from the syringe, can be controlled from the Krüss software.

- The illumination can be adjusted to obtain a good contrast between the drop and the surface, which assists the program in determining the profile.

- The magnification can be changed by the zoom lens to obtain the best image of the drop.

- Multiple software options exist for determining the contact angle from the droplet profile. These include tangent methods and profile fitting methods.

.

3.6.1 System calibration

The syringe was placed in the syringe holder. Its image was centred in the screen. The focus was then adjusted to obtain the optimal view of the needle. The needle (supplied by Krüss) has a known diameter, which was used to calibrate the image.

3.6.2 Methods of contact angle measurement

The Krüss software uses five different methods for calculating the contact angle. All of them calculate the contact angle as $\tan\theta$ at the intersection of the drop contour line with the surface line (base line). The five methods are [13]:

1. Tangent method 1, in which the complete profile of a sessile drop is adapted to fit a general conic section equation. The derivative of this equation at the intersection point of the contour line with the base line gives the slope at the 3-phase contact point and therefore the contact angle.

2. Tangent method 2, in which a part of the profile, which lies near the base line is adapted to fit a polynomial function of the type

$$(y = a + bx + cx^{0.5} + d / \ln x + e / x^2)$$

The slope at the 3-phase contact point at the base line and from it the contact angle is determined using iteratively adapted parameters.

3. Height width method, in which the height and width of the drop are determined first, and then the contact angle is calculated from the contour line, regarded as a segment of a circle, enclosed by a rectangle.

4. Circle fitting method, in which the contact angle is calculated from fitting the drop contour to a circular segment function.

5. Young-Laplace (sessile drop fitting), in which the contact angle is calculated from fitting the complete drop contour to a Young Laplace equation.

The method used mostly in this study was Tangent method 1, because visually it gave the best fit of drops of contact angle greater than 150°. Figure 3.5 shows the different fits of the drop profile offered by the Krüss software.
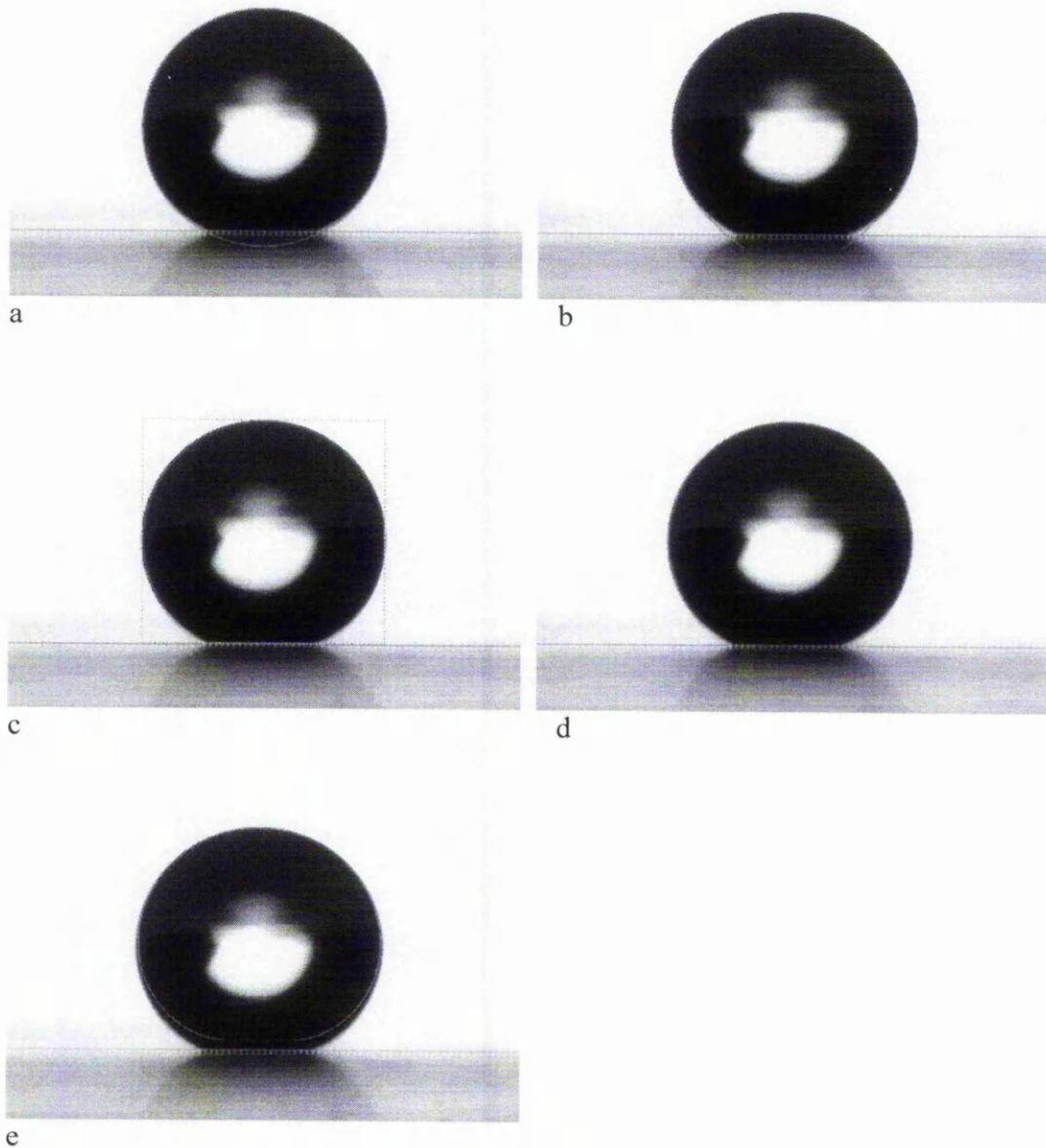
Figure 3.5. Contact angle measurement using the five different methods offered by the Kruss software: **(a)** Tangent Method 1 **(b)** Tangent Method 2 **(c)** Height and width method **(d)** circular fitting **(e)** Young Laplace equation.

3.6.3 Static contact angle measurement

To measure the contact angle of water on patterned hydrophobic surfaces, the drop was first deposited gently. It was given a few seconds to equilibriate and then a snapshot of the drop was acquired, which was then analysed using Krüss drop shape analysis software. The drop base line was determined manually and then tangent method 1 was used to calculate the contact angle. In this method the complete profile of the sessile drop is adapted to fit a general conic section equation. The derivative of this equation at the intersection point of the contour line with the base line gives the slope at the three phase contact point and therefore the contact angle [13].

3.6.4 Dynamic contact angle measurement

The contact angles of drops advancing or receding (during spreading or evaporation respectively) were measured using Krüss drop shape analysis software. The base line was determined manually and then a function called (calculate) was used. This function in the Krüss software allows the calculation of the drop contact angle as a function of time, as well as other drop parameters such as volume, surface area, base diameter and height. The software assumes axial symmetry in the droplet shape. The data was then transferred to an excel file for analysis.

3.6.5 Contact angle hysteresis measurement

Measurements of hysteresis for droplets on superhydrophobic surfaces can present difficulties not encountered with other surfaces. Here we report on the methods used in this study to estimate the contact angle hysteresis and their limitations.

Method 1 is the tilting stage method shown in figure 3.6. In this method the drop is deposited on a horizontal surface and the stage is then tilted. When the upper and lower contact angles of the drop reach the minimum receding angle and maximum advancing angle, the drop will move. In principle, measuring the hysteresis in this manner appears to be straightforward. This was not the case for many drops. A drop of configuration corresponding to Wenzel, doesn't move, and stuck to the surface structure. Therefore tilting method is not suitable for such a measurement.
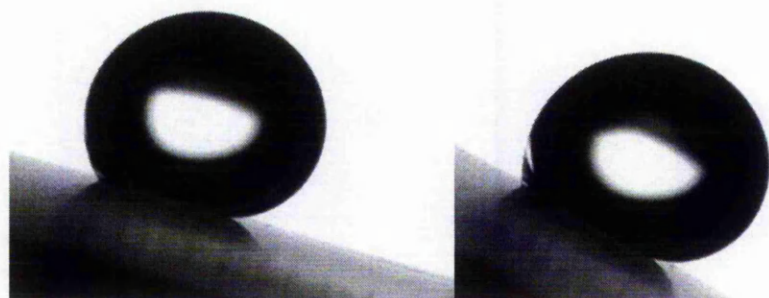
Figure 3.6. Measurement of the advancing and receding angle using the tilt method. As the substrate tilt angle increases the drop starts to move, indicated here by the bright shadow in the trailing portion of the drop.

Method 2 is by adding or withdrawing liquid to measure the advancing or receding angle, respectively. If the needle is left in the drop while adding or withdrawing, then needle pressure can present external forces that spoil the measurement by causing drop shape distortion (see figure 3.6). If, on the other hand, the drop is detached from the needle after adding or withdrawing liquid, then that external force exerted to detach the drop will have an effect on the contact angle. Figure 3.7 shows a drop (with configuration corresponding to Cassie) during liquid addition. In the first panel, the drop couldn't be detached from the needle, because the surface is very hydrophobic. As the drop volume is increased, the contact angle decreased (contrary to what one expects). This is because the contact diameter increased and couldn't be controlled. A finer needle is needed, which has to be capable of pumping smaller amount of liquid. The effect of the presence of needle can be seen in figure 3.7. by comparing the values of the contact angles in c and d. the volume of the drops in c and d is equal, but the values of the contact angles are 151° and 145° respectively. The distortion of the drop shape due to the needle presence is obvious

therefore measuring the advancing contact angle with the needle inside the drop is not reliable.

Receding contact angle measurement on the same kind of surfaces (Cassie) was not possible, because withdrawing liquid from the drop results in the drop coming off the surface.
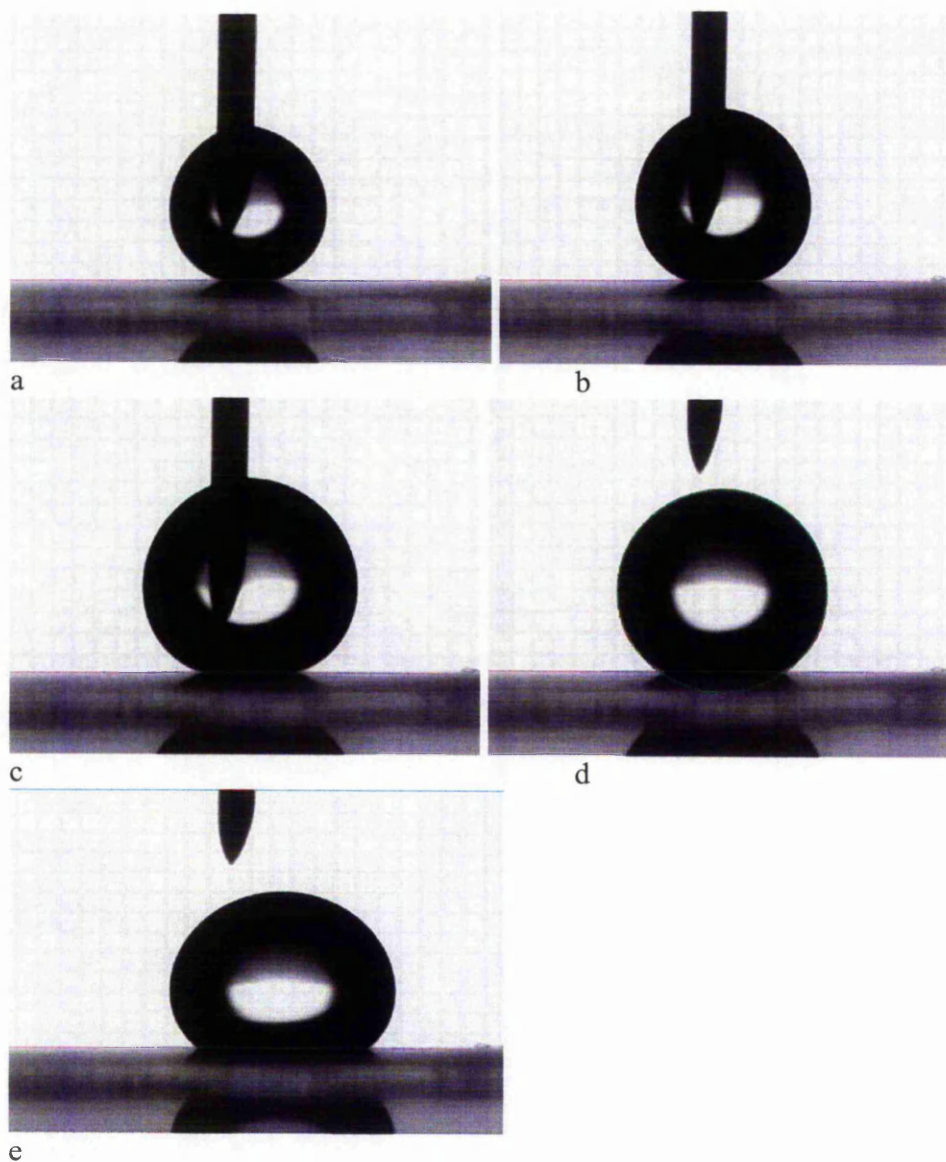
Figure 3.7. Measurement of the advancing contact angle by adding liquid. In (a) the drop couldn't be detached from the needle because it is very small (~1.48µL), in (b) the volume is increased to ~2.44µL, which results in contact angle of 153.6°. Further increase in the drop volume (c) causes decrease in the contact angle to 151°, when the drop is detached from the needle (d) the contact angle drops to 145°. In (e) the drop collapsed two seconds after the detachment to the Wenzel contact angle.

Method 3 is moving a drop across the surface. In this method the drop is dragged by the needle to its right or left side (figure 3.8), which causes it to move across the surfaces and jump from one pillar to the next on the patterned surface. The angles just before the drop jump provide an estimate of the advancing and receding angles. This method was applicable to drops sitting on an air-solid composite surface (Cassie type). Otherwise dragging the needle through the drop causes drop spreading.
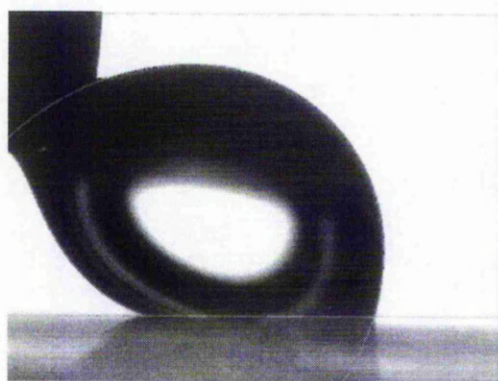
Figure 3.8. Estimating the advancing contact angle by dragging the drop to one side.

The methods that can be used to estimate the hysteresis with drops on superhydrophobic surfaces depends upon the surface and the state of the drop. Because there is no proof that these three methods of estimating hysteresis provide theoretically equivalent advancing and receding contact angles, this thesis report the methods used along with the values obtained. The work in this thesis uses the estimates of hysteresis as an aid to identify weather a Cassie or a Wenzel state is occurring rather than to provide absolute value of advancing and receding contact angles.

3.7   Experimental setup

3.7.1 Spreading experimental setup

Many spreading studies (including this study) have been done using a non-volatile viscous oil to avoid evaporation, which complicates data interpretation due to the volume change. Moreover the spreading rate can be controlled by choice of viscosity whilst maintaining a relatively constant surface tension. The liquid used in this study was polydimethylsiloxane (PDMS). It is a silicone oil providing complete wetting of most surfaces. The viscosity and density used in this work were 10000 centistokes and 0.98 gm/cm^3, respectively.

To study the spreading of PDMS on patterned surfaces, a drop of size about 1 microliter was deposited gently using a needle. To keep the whole drop visible during various stages of spreading, the zoom was adjusted at the beginning. The needle and the surface were also adjusted so that their images were in the centre of the screen. The Krüss DSA10 was used to record the process. A number of frames were recorded with a narrow time gap at the beginning, and a wider time gap towards the end of the process; the spreading is a power law in time. For example in the first 15 seconds a frame was acquired every 2/25 seconds, followed by a frame every 1/5 seconds for 20 seconds and finally a frame every 10 seconds. The number of frames acquired needed to follow the whole spreading process was adjusted before starting recording. The experiments were performed at room temperature conditions.

3.7.2 Evaporation experimental setup

The evaporation of small water drops on patterned surfaces was conducted in a shielded area to keep it free from dust and air currents. The experiments were performed at room temperature and humidity (which were recorded). The needle was adjusted so that its image was in the centre of the screen. The drop was deposited carefully to try to avoid it being forced into the surface structure, which sometimes was unpreventable.

Room temperature evaporation of water drops on a patterned surface is a slow process. A two microliter drop takes more than 15 minutes to evaporate at room conditions. For this reason the recording system was adjusted to acquire a number of frames. In the first minute a frame per second was acquired to capture the moment the drop is deposited on the surface. This was done because some drops collapsed into the surface during deposition or a short while after deposition. The time gap between the frames was then increased to be 10 seconds. Towards the end of the drop life time the gap was 5 seconds. The temperature and humidity were recorded.

This chapter has described the experimental methods and arrangements used in this thesis. A method for producing patterned surfaces (photolithography) was discussed in detail as well as methods of surface characterization. The contact angle hysteresis measurements methods were also described and limitations discussed. The experimental arrangements used for studying spreading and evaporation of droplets from the patterned surfaces were discussed. In the following two chapters, the results obtained from photolithography, electrodeposition and contact angle measurement on patterned surfaces are presented as well as data of spreading and evaporation on the patterned surfaces.

References:

1. N Shirtcliffe, S. Aqil, C. Evans, G. McHale, M. I. Newton, C. C. Perry, P. Roach, *Journal of Micromechanics and Microengineering*, 14, **2004**, 1384.

2. www.ece.gatech.edu/research/labs/vc/theory/photolith.html.

3. A. Tselev, K. Hatton, M. S. Fuhrer, M. Paranjape, P. Barbara, *Nanotechnology*, 15, **2004**, 1575.

4. M. Nathan, O. Levy, I. Goldfarb, A. Ruzin, *Journal of Applied Physics*, 94, **2003**, 7932.

5. K. Elgaid, D. McCloy, I. Thayne, *Microelectronic Engineering*, **2003**, 67–8, 417.

6. C. Malek, *Microelectronic Journal*, 33, **2002**, 101.

7. http://www.geocities.com/guerinlj.

8. R. Feng , R J Farris, *Journal of Micromechanics and Microengineering*, 13, **2003**, 80.

9. www.microchem.com.

10. N. Shirtcliffe, G. McHale, M.I. Newton, C. C. Perry, *Langmuir*, 21, **2005**,3.

11. JSM-840A manual.

12. M. -Z. Zhang, M. Wang, Z. Zhang, J-M. Zhu, R. -W. Peng and N. -B. Ming *Electrochimica Acta*, 49, 14, **2004**, 2379.

13. G. McHale, H. Y. Erbil, M. I. Newton, S. Natterer, *Langmuir*, 17, **2001**, 6995.

14. Krüss manual, Krüss GMBH, Hamburg, **2002**.

Chapter 4

Results and discussion 1

Wetting static and dynamic

4.1   Introduction

This chapter begins by presenting samples of patterned and rough surfaces produced by photolithography and electrodeposition respectively. It then characterizes their hydrophobicity. The wetting of the patterned surfaces (produced by photolithography) is then described. Three effects were observed, the first is enhancement of the non-wetting (hydrophobic and superhydrophobic) properties, the second is transformation from a partial wetting regime with contact angles less than 60° to a complete wetting regime, and the third is enhancement of the dynamics of a complete wetting regime.

4.2   Photolithographic surfaces

Photolithography is a time consuming process. In order to find out the optimum recipes for each pattern, the process was repeated many times. One of the aims of this study was to develop the photolithographic technique to a reliable and reproducible method of fabricating patterned surfaces. The major challenge was to obtain pillars with vertical walls and high aspect ratio (defined as pillar height divided by its diameter). The small pillars, those with diameter and separation less than 10 μm, were more susceptible to fall over during developing due to their mushroom like shape as seen in figure 4.1. Here the pillar diameter and separation are designed to be 8 μm each. However, following fabrication the bases of the pillars are narrower than the tops, making them very weak.
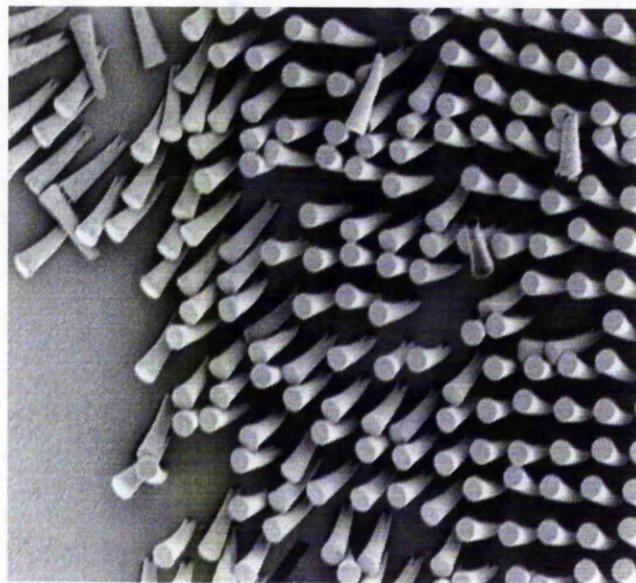

Figure 4.1. Scanning electron microscope image of the 8-μm pillars, which fall over during developing.

Not all of the mushroom like pillars falls. Figure 4.2 shows small pillars (about 8 µm in diameter), which didn't fall over because the separation is greater than the diameter.
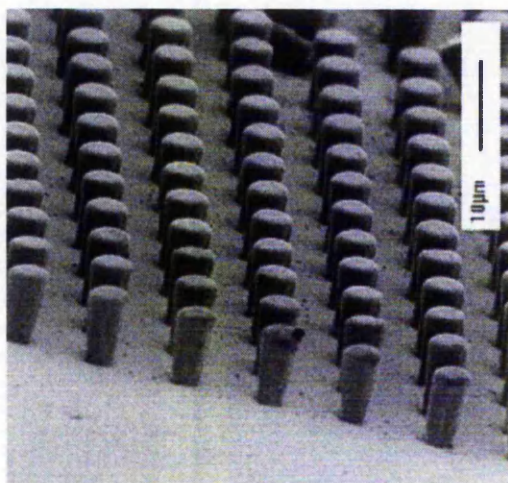

Figure 4.2. Scanning electron microscope image of mushroom like pillars which didn't fall over because they are separated by a greater distance.

This problem was solved by exposing the photoresist SU-8 50 to the UV through a filter [1]. A sheet of ¾ C. T. blue filter (Lee filters, UK) was used to cut out wavelengths shorter than 250 nm. This is because the mercury lamp used to produce UV has 4 peaks: two under 250 nm (which were cut using the filter, one above 400 nm one (we didn't take any precautions because the SU8 is insensitive above 400nm), and the one needed to cause cross linking (hardening of the photoresist). Because the exposure was done through a mask with open (transparent) circles patterns arranged in a square lattice, the resultant pattern were cylindrical pillars of diameter equal to the mask circle diameter. The diameter of the pillars however was not always equal to the mask circle diameter. Over-exposure usually results in wider pillars (than the mask circle diameter), while under-exposure results in pillars of smaller

diameter than the mask circles. All the patterned surfaces used in this study were created on a flat layer of SU-8 50 to ensure chemical homogeneities of the patterned surfaces (pillars and the area in between). This flat layer also improves the adhesion of the pillars to the surface. Patterns of different sizes and depth were obtained. Figure 4.3 shows two patterned surfaces with aspect ratio greater than 3, near vertical side walls and well-defined shapes.
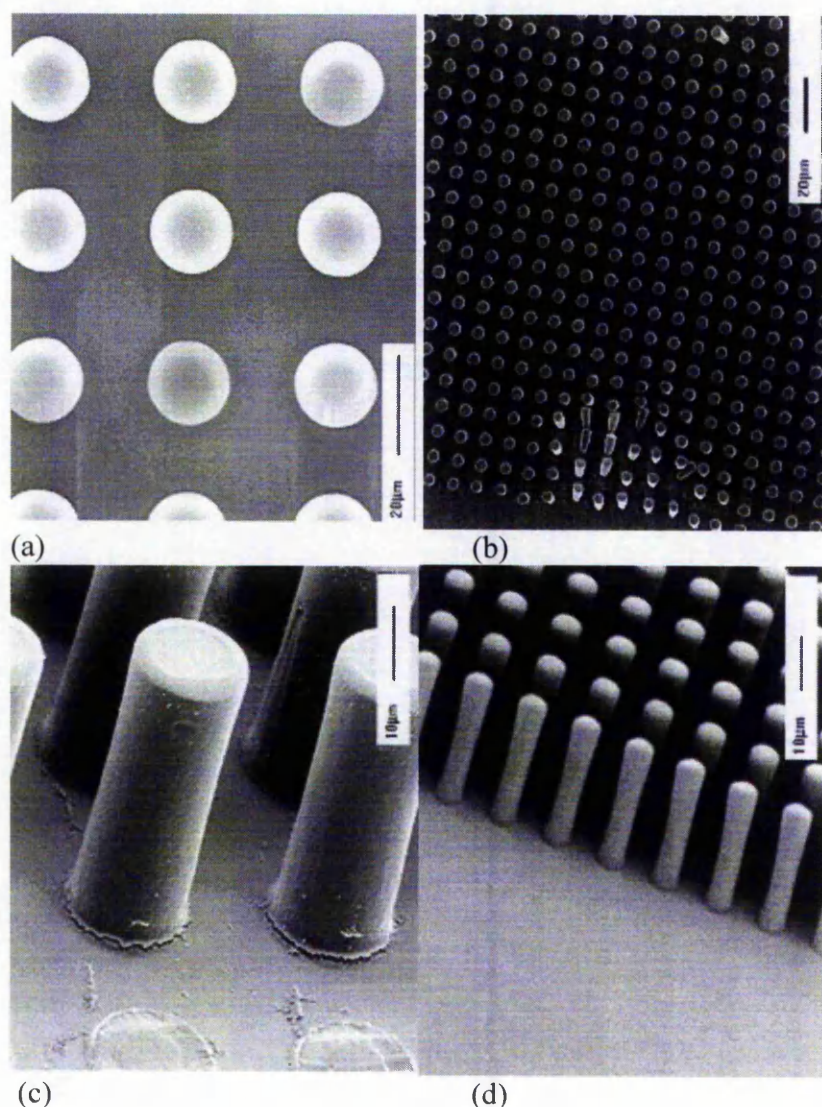

(a)   (b)   (c)   (d)

Figure 4.3. Scanning electron microscope images (top and side view) of the 15 μm pillars (a,c) and 4 μm pillars (b,d).

4.3   Electro-deposited surfaces

The focus of this study is investigating the wetting properties of geometrically structured surfaces. However other techniques can be used to produce rough surfaces which can be used in studying the relationship between wetting and surface topography. One of these developed during this work was copper electro-deposition, which was shown to produce a randomly rough surface. Figure 4.4 shows a side view of a rough surface produced by copper electro-deposition. The current density used here is 300 mA/cm^2 and the deposition time was 3 minutes. Figure 4.5 shows a droplet of water on that surface. Contact angle measurement on such a surface is difficult due to difficulties in assigning the droplet base line.
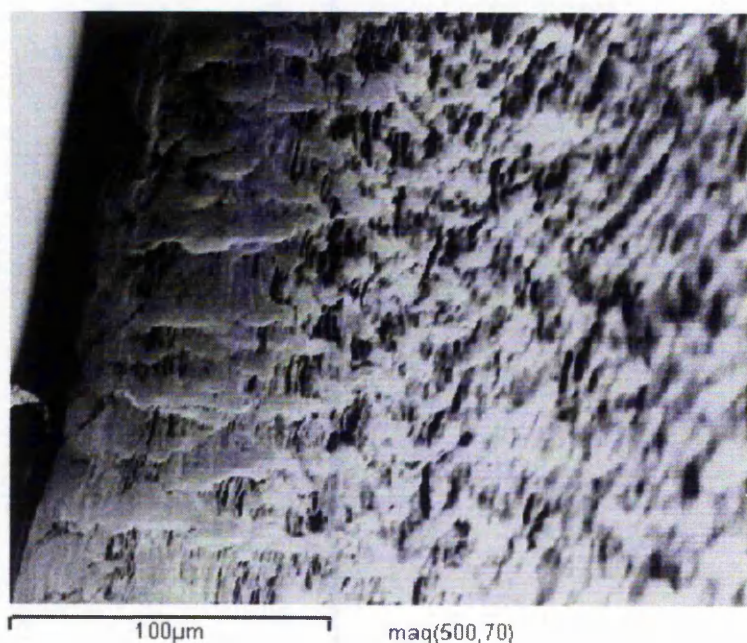

100μm   mag(500,70)

Figure 4.4. Scanning electron microscope image of electrodeposited surface. The sample is tilted to 70°.
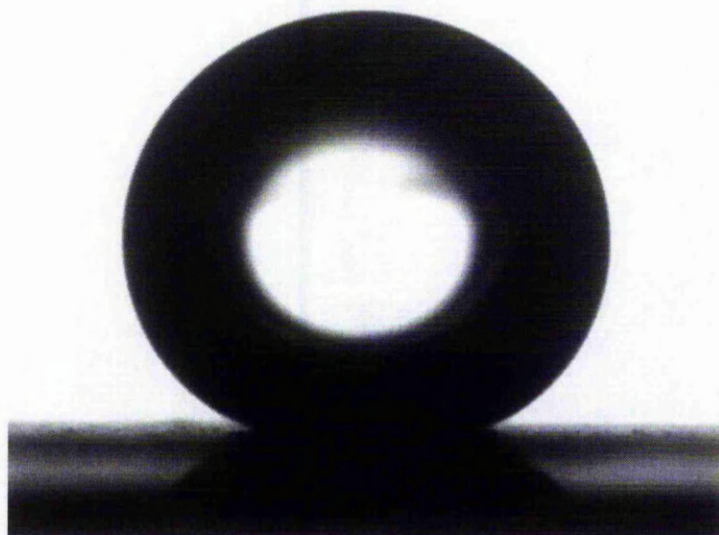
Figure 4.5. A droplet of water on a surface produced by electro-deposition.

4.4   Water contact angle on patterned surfaces

To characterize the hydrophobicity of the patterned surfaces produced by photolithography, the contact angle of water was measured. These patterned surfaces are shown to be hydrophobic and even superhydrophobic. Figure 4.6 shows a high contact angle (153°) obtained on one of the patterned surfaces with diameter, separation and height equal to 11.5, 18.5 and 25 µm respectively. Light can be seen to penetrate between the pillars which show that the liquid did not penetrate the pattern, and the drop is sitting on a composite solid-vapour surface (Cassie-Baxter type). Assigning the contact line presents a difficulty on these types of surfaces because of the pillars. The contact line was placed on the top of the pillars, assuming that the Cassie drops don't penetrate the surface at all. This may not exactly be true since a kind of curvature may develop below the drop as described in the model in figure 4.7. Using tangent method 1, and when placing the base line at the bottoms of the pillars rather than the tops, the contact angle that is measured is found to be slightly different. The difference is about one degree (higher when the base line is at the bottom of the pillars).
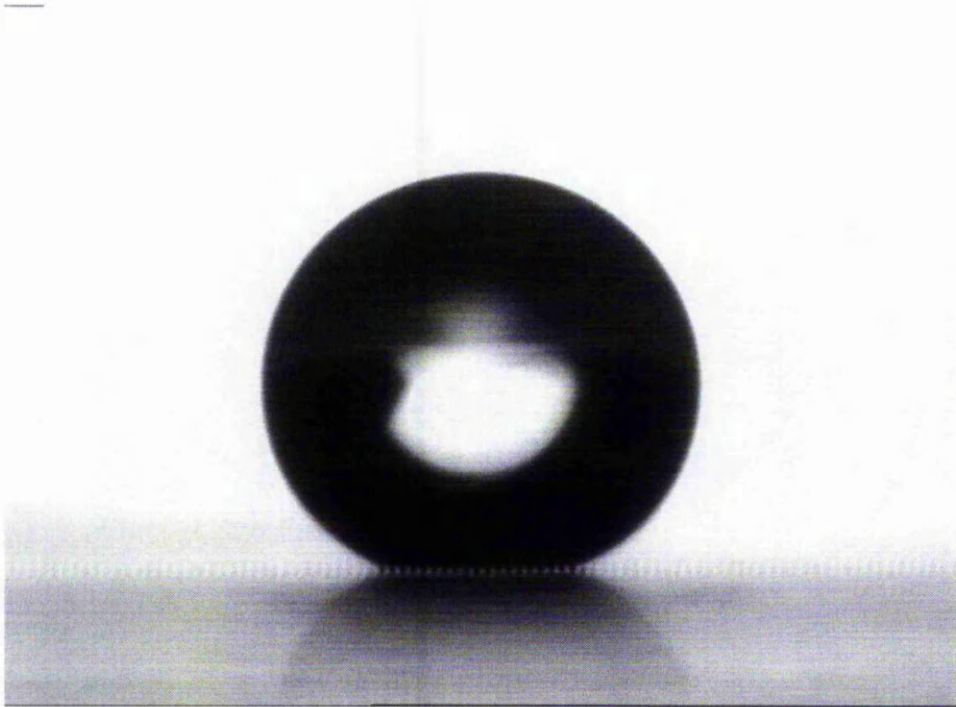
Figure 4.6.   A droplet of water contact angle of 153° obtained on a patterned surface of diameter-separation-height measured to be 11.5, 18.5, 25 μm respectively.
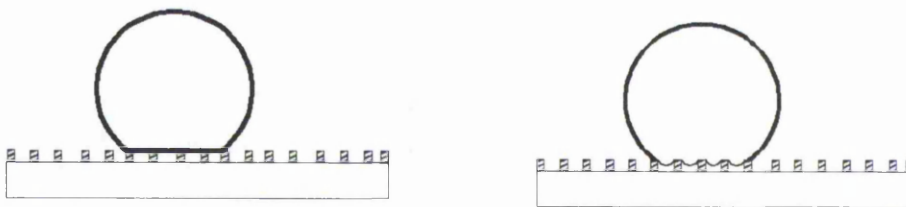
Figure 4.7.   The left hand side of this figure presents Cassie Model (a drop suspended on pillars), the right hand side may be the real shape of the drop base, where a curvature is developed in the gaps of the pattern. This partial penetration could be due to the drop weight or because the pattern acts as connected capillary tubes. From a theoretical point of view no penetration is possible if the pattern is in the form of isolated capillary tubes.

In a systematic study of the effect of pattern height on the apparent contact angle, samples of diameter equal to 15 μm separated by 15 μm were fabricated. Their heights range from 0 to 70 μm. Table 4.1 displays

the results. The first column is the pillar height; the second is the contact angle due to surface structure only, while the third is the combination effect of the surface structure and the hydrophobizing agent (flutec solution). The contact angle of the flat surface is also reported for comparison. The general observation is that the contact angle initially increases with patterned height but then saturates. The highest contact angle obtained on these surfaces was 143° and 149° for the unhydrophobized and the hydrophobized surface respectively. The expected Cassie angle on these surface (of φ_s=0.196) were 140.3° and 152.4° not far from the experimental results shown in table 4.1. It should be noted that if the pattern produced by photolithography is slightly different from the designed value (say pillars of diameter of ±o.5 μm) then the expected Cassie angle is ±1.4°. This could be a cause for getting different contact angle on the pattern sample selected here. The results may reflect the contact angle hysteresis on that kind of surfaces.

Pillars height (µm) (±5% of pillars' height)	Contact angle on untreated patterned surface(°) ±2°	Contact angle on hydro-phobized patterned surface (°) ±2°
Flat layer of Su8-50	80	114
6	100	117
10	102	120
26	142	149
45	141	148
70	143	149

Table 4.1. Water contact angle on structured surfaces with the same pillar diameter and separation (15 µm) but with different heights.

The contact angle on surfaces of the same diameter and separation were measured and these are reported in ref. [1]. It is shown that the contact angle increases as the pattern height is increased and reaches saturation at some height. At this height the drop may penetrate the patterned surface or be suspended over the pillars, depending on the drop deposition method (forced or gentle deposition). Above that height the drop prefers suspension (i.e. Cassie-Baxter type). Contact angle maximum of 143° and 145° were obtained on these patterned surfaces for the unhydrophobized and hydrophobized samples respectively. For these particular patterned surfaces (of diameter and separation equal to 15µm) the critical height was around 10 micron. The results are plotted in figure 4.8.
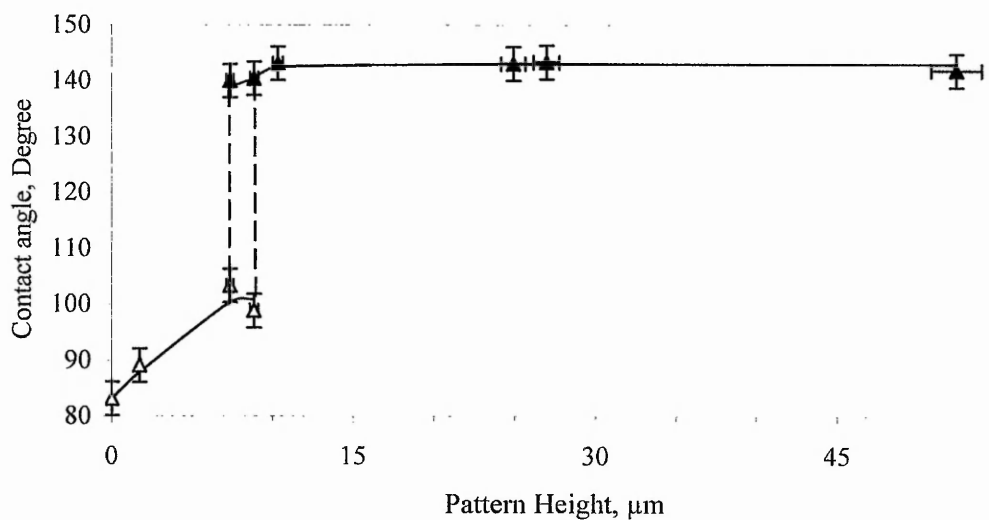
(a)
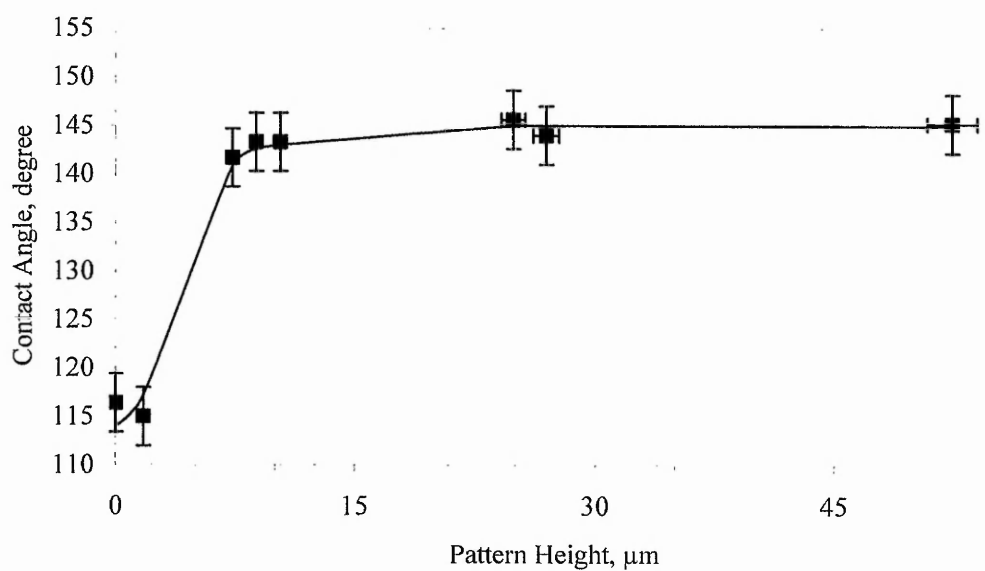
(b)

Figure (4.8). Water contact angle on patterned surfaces with different heights, (a) unhydrophobized, (b) hydrophobized. Ref. [1].

The possibility of having either Wenzel or Cassie-Baxter drop on a patterned surface has been studied extensively in the last few years [2-7]. The available energy during deposition determines whether the drop will follow the surface topography or sit on a composite surface [3]. Condensing a droplet onto a surface from the vapour phase usually results in a Wenzel case [4], depositing it on a surface by a needle may result in either Wenzel or Cassie-Baxter type. Transition from a Cassie-Baxter state to a Wenzel state can be induced by applying pressure. Relaxing the pressure will not result in a Cassie-Baxter drop, which means that the transition is irreversible [4].

4.5 Effect of surface structure on partial wetting

A surface is partially wet if a small quantity of liquid forms a droplet of a contact angle of some value between 0 and 180°. Roughness is known to alter the wettability of the surface in both directions. It may decrease or increase the contact angle according to the Wenzel equation [8,9]. Patterning the surfaces was shown in the previous section to causes transition to a non-wetting state and even causes surface superhydrophobicity (which is defined as surface with contact angle greater than 150°). On the other hand transition from partial wetting to complete wetting has also been obtained on these patterned surfaces [9]. A range of liquids, which are known to form a drop of finite contact angle on the smooth surface made from the polymer SU-8 50, were deposited on the SU-8 50 patterned surface and their contact angles were measured. The results are shown in table 4.2; liquids of contact angles

less than 51° on the smooth surface do not form a droplet when deposited on the patterned surfaces [9].

Liquid	γ_{LV} (mN/m^2)	Contact angle on flat surface(°)	Contact angle on patterned surface(°)
PDMS	21,2	0	0
Octane	21,8	3	0
Diiodomethane	50,8	23,7	0
PEG 200	43,5	38	0
Ethylene Glycol	47,7	51	0
Formamide	58,3	61,5	30
Glycerol	63,7	70	109
Water	72,8	80	145
Mercury	465	162	167

Table 4.2. Effect of surface structure on partial wetting regimes. The pillars diameter, separation and height are 15, 15 and 45µm respectively.

4.6 Dynamic wetting

The effect of surface topography on the dynamics of wetting was studied by following droplets of PDMS oil spreading on a patterned surface. PDMS (polydimethylsiloxane) was chosen because it is a non-volatile oil with wide range of viscosities available for the same surface tension; a viscosity of 10,000 cSt was chosen so that the spreading should occur over timescale of

minutes to an hour. The size of these droplets was less than the capillary length so that the spreading is mainly derived by the surface tension forces [10]. From the side-profile images of the drop, the volume, base diameter and dynamic contact angle were determined as a function of time using the Krüss drop shape analysis software.

A typical behaviour of a PDMS drops' contact angle on patterned surface is shown in figure 4.9; the figure also shows the drop contact angle on a flat surface. The steeper slope of the patterned surface indicates a faster spreading regime.
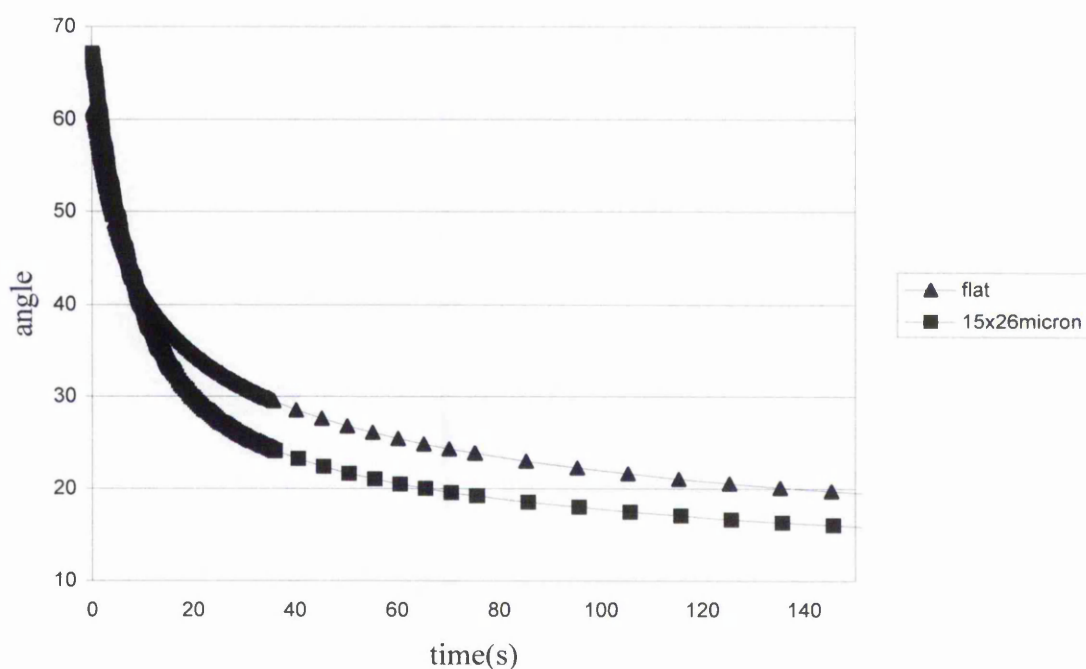

Fig. 4.9. Angle versus time curves for the flat (▲) and structured surface (■) with pillar diameter of 15 μm and height of 26 μm.

The drop volume remains constant over most of the spreading time, but the final stage of the spreading was characterized by draining of the drop into the surface structure. For the constant volume period, the theoretical modifications of spreading dynamics on these patterned surfaces suggested by McHale and Newton [11] were examined for a number of surfaces of diameter 15 micron. These surfaces have different height ranging from 0 to 70 μm. The spreading experiments were repeated at least five times for each pillar height to assess reproducibility of the results. Figures 4.10-4.12 are representative samples of a much greater set of data, which is then summarized in figure 4.13.

4.6.1   Contact angle-time relationship

Tanner's law [13] indicates that the contact angle variation with time for a drop spreading on a flat horizontal surface follow the simple power law $\theta \propto \dfrac{1}{t^n}$, where n =0.3. McHale and Newton [11] claim that the spreading of a drop on a rough surface will still follow a simple power law but with a higher value for the exponent n. To check their prediction the data for spreading on lithographically structured surfaces was used to calculate the n. For accurate calculation of n, the contact angle was calculated from fitting the data to the equation $\theta = \dfrac{a}{(t+c)^n}$, where a, c and n are fitting variables; the Excel function "Solver" was used to obtain the fit. The constructed curve (by Solver) fitted the actual experimental data, up to the point where the volume conservation broke down. For the constant volume period, n was calculated from the log-log plot

of the contact angle-time data. Figure 4.10 shows a sample of the full data set

obtained plotted on a log-log plot and the fit constructed by solver (left hand

axis). The variation of volume with time is also plotted (right hand axis). The

latter curve was used to find the cut-off point when the droplet volume is no

longer approximately constant due to liquid draining into the pattern. This point

was selected so that the volume loss is less than 2% of the initial drop volume

and the measured and calculated logarithm of the contact angle no longer fit

each other. For this particular patterned surface n is equal to 0.71, indicating

faster spreading.
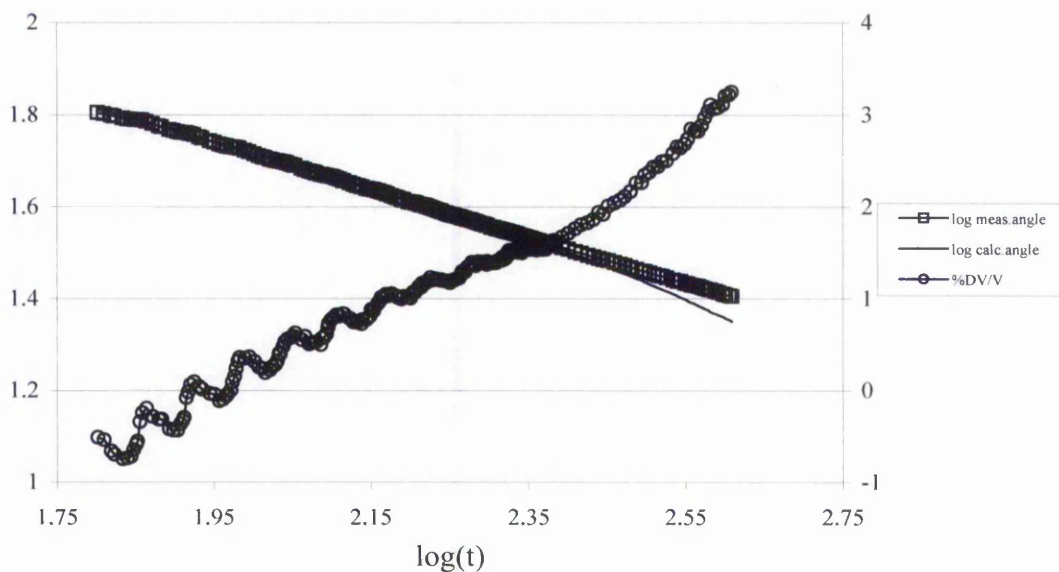
Figure 4.10. The measured and calculated dynamic contact angle-time relationship on a log-log scale (The left hand side y-axis is the logarithm of the contact angle) for the structured surface with pillar diameter of 15 μm and height of 26 μm; the volume variation (multiplied by -1) with time is also plotted on the right hand side axis. The volume oscillation is due to the stick-slip motion of the drop, which is found to bridge the gaps between the pillars in the early stages of spreading (imagine the drop edge slightly penetrating the small gap (volume loss) between the pillars before bridging the gap (becoming again part of the drop spreading just above the pillars) i.e above the base line.

4.6.2   Base diameter-time relationship

The drop base diameter can also be used to evaluate drop spreading. On a horizontal flat surface the drop base diameter variation with time follows a power law $d \propto t^{m}$. Tanner [13] estimated m to be 0.1. The data for the change in base diameter with time for each of the rough surfaces used in this study were plotted on a log-log scale, and the exponent m of the power law of drop spreading was calculated using Solver. Figure 4.11 shows the measured and calculated base diameter against time (left hand axis); the volume variation with time is also shown on the plot (right hand axis). For this particular figure (15x26 µm), the exponent m is 0.2, indicating a faster rate of spreading.
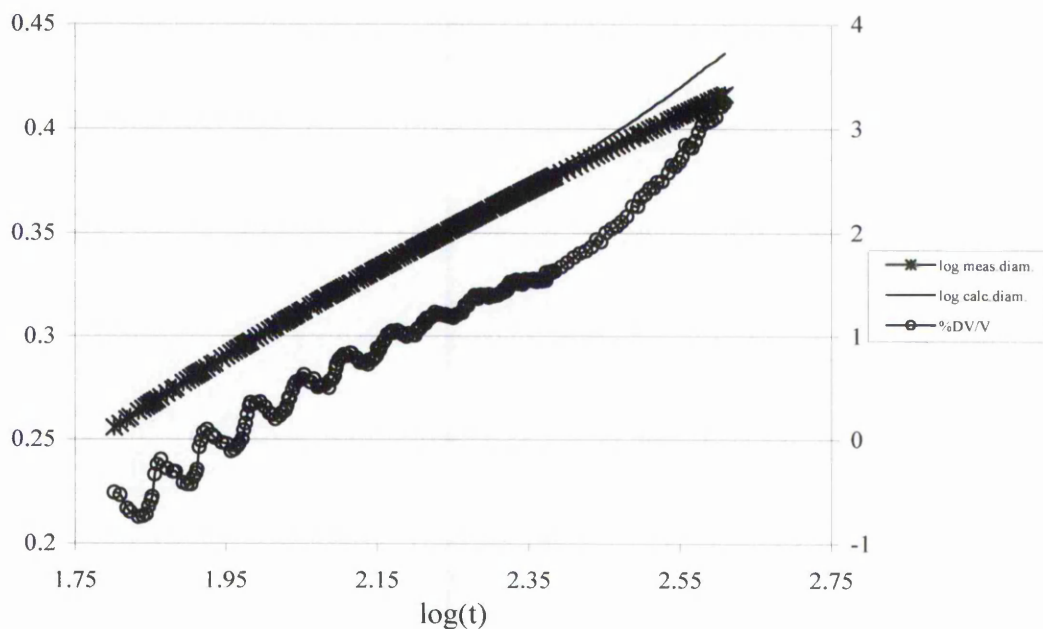

Figure (4.11). The measured and calculated drop base diameter-time relationship on a log-log scale for the structured surface with pillar diameter of 15 µm and height of 26 µm. The left hand side y-axis is the logarithm of the drop base diameter, and the right hand side y-axis is the volume variation multiplied by -1.

4.6.3   Edge velocity-contact angle relationship

Hoffman's [14] experimental data showed that for a drop spreading on a horizontal flat surface, the relation between the drop edge velocity and the dynamic contact angle is $v_{E} \propto \theta^{p}$, where p is equal to 3. To determine the power p for a drop spreading on a patterned surface, the drop edge velocity was first calculated from the rate of change of the base diameter and was then plotted against the dynamic contact angle on a log-log scale as shown in figure 4.12 for one of the structured surfaces (the 15 μm diameter cylindrical pillars with height of 26 μm); the smooth surface data are also plotted for comparison. The obvious oscillation in the edge velocity is caused by the stick-slip motion of the drop edge. Analysis of the oscillations in the edge speed indicates that successive maxima and minima correspond to changes in contact diameter of the drop equal to the lattice parameter (i.e. 30 μm) reflecting the lattice of the pillars. The average slope of this particular edge velocity-dynamic contact angle curve is 1.58, indicating that the velocity tends to a linear function in the contact angle on the structured surface rather than cubic which is the case for the flat smooth surface.
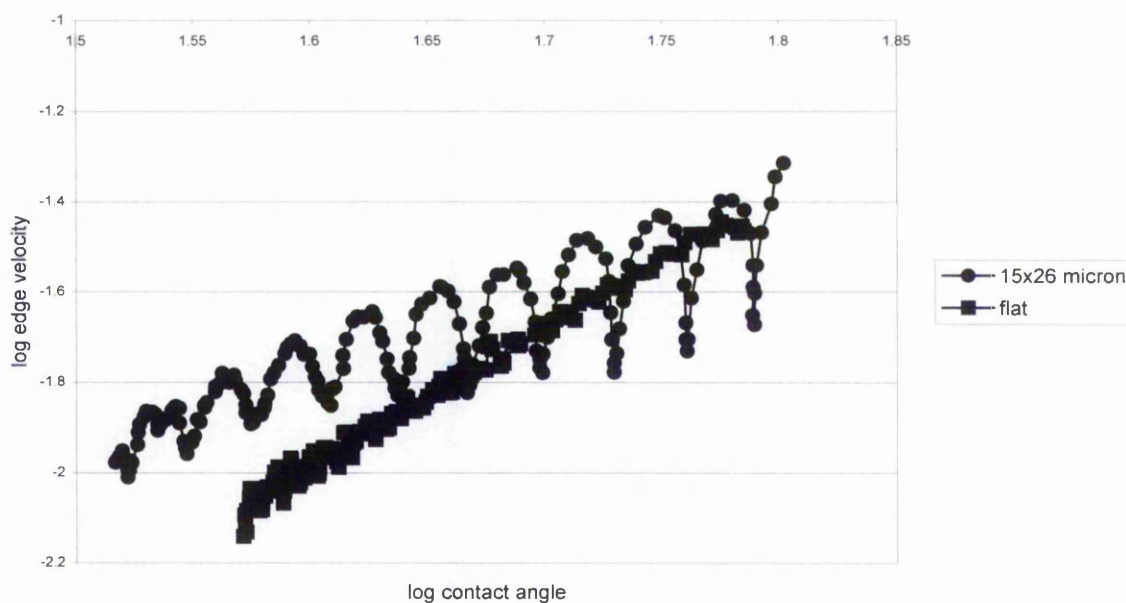
Figure 4.12. Edge velocity-dynamic contact angle relationship on a log-log scale for the smooth and structured surface for the structured surface with pillar diameter of 15 μm and height of 26 μm.

4.6.4   Spreading power versus pattern height

The effect of pattern height on the power law of spreading is summarized in figure 4.13 [12]. The figure shows the exponent n (determined using the contact angle-time data) and the exponent p (determined using the edge speed-contact angle data) as a function of the pattern height. As the pillars' height increase the n changes from 0.3 (equation 2.28) towards 0.75 (equation 2.42) as predicted. The exponent p also shows a change from $p=3$ (equation 2.34) to $p=1$ (equation 2.41), i.e. a trend from cubic to linear function.
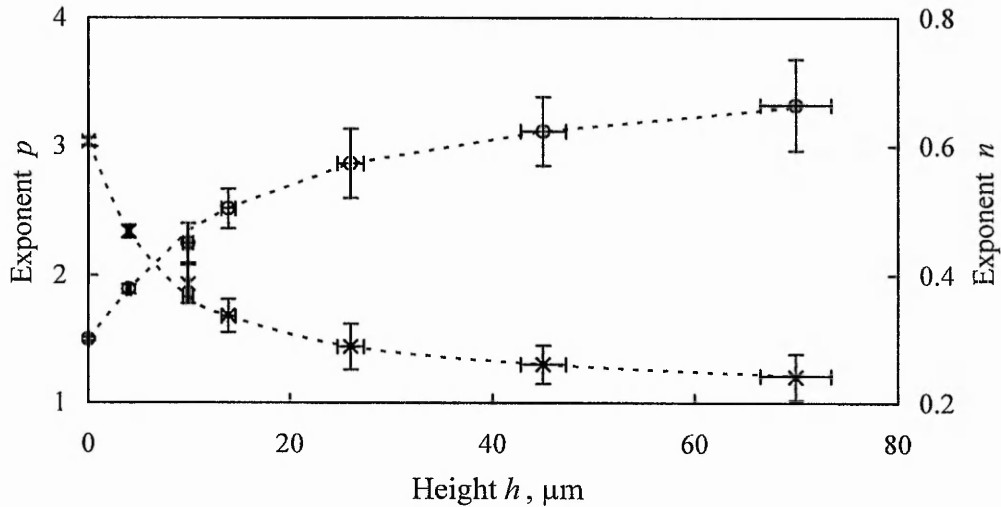
Figure 4.13. Exponent *p* extracted from the edge speed-dynamic contact angle (xxx) for spreading of PDMS on patterned surfaces; the dotted curve indicates the trend from cubic to linear form with increasing pillar height. The variation of the dynamic contact angle-time exponent *n* (ooo) with pillar height is indicated by the right hand axis. The dotted curve indicates the trend from 0.3 to o.75 with increasing pillar height [12].

Additional data for PDMS oil spreading on a naturally occurring hydrophobic surface of water contact angle of 165° (a sprout leaf of *brassica oleracea*) resulted in an exponent p ~2, indicating superwetting driven by the surface topography [12].

4.7   Spreading of the precursor film

This study dealt with the spreading of drop on the macroscopic scale. However the precursor film spreading on one microstructured surface was viewed using the confocal microscope. In figure 4.14 the oil film is advancing to the left. The figure shows that film moves first towards the pillars probably indicating superwetting driven by surface topography. It should be mentioned that this picture was obtained few hours after recording the macroscopic drop spreading.
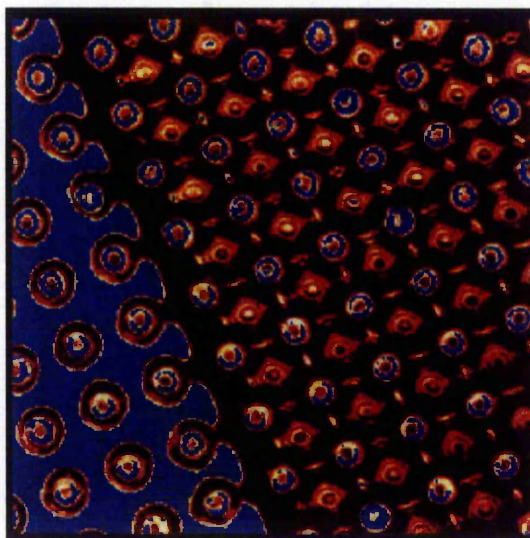
Figure 4.14. The spreading of the precursor film on a patterned surface. The blue area at the left is not invaded yet by the precursor film, which seems to be moving towards the pillars, probably indicating superspreading driven by surface topography.

In this chapter, the three effects of the surface structure have been demonstrated:

1. Transition of water droplets to a superhydrophobic or non-wetting state.

2. Transition of liquid droplets from partial wetting to complete wetting.

3. Speeding the spreading of complete wetting liquids.

In the following chapter, the effect of surface structure on the evaporation process is presented.

References

1. N. J. Shirtcliffe, S. Aqil, C. Evans, G. McHale, M. I. Newton, C. C. Perry, P. Roach, *Journal of Micromechanics and Microengineering,* 14, **2004**, 1384.

2. W. Extrand, *Journal of Colloid and Interface Science,* 248, **2002**, 136.

3. N. A. Patankar*, Langmuir,* 19, **2003**, 1245.

4. A. Lafuma, D. Quere, *Nature,* **2003**, 457.

5. J. Lee, N. A. Patankar, B. He, *Langmuir,* 19, **2003**, 4999.

6. D. Quere, A. Lafuma, J. Bico, *Nanotechnology,* 14, **2003**, 1109.

7. N. A. Patankar, *Langmuir,* 20, **2004**, 7097.

8. R. N Wenzel, *Industrial Engineering Chemistry*, 28, **1936**, 988.

9. G. McHale, N. Shirtcliffe, M. I. Newton, *Analys,t* 129, **2004**, 284.

10. P. G. de Gennes, *Review of Modern Physics,* 57, **1985**, 827.

11. G. McHale, M. I. Newton, *Colloids and Surfaces (A),* 206, **2002**, 193.

12. G. McHale, N. J. Shirtcliffe, S. Aqil, C. C. Perry, M. I. Newton, *Physical Review Letters,* 93, **2004**, article 036102.

13. L. H. Tanner, *Journal of Physics, Applied Physics*, 12, **1979**, 1473.

14. R. Hoffman, *Journal of Colloid and Interface Science,* 50, **1975**, 228.

Chapter 5

Results and discussion 2

Evaporation from a superhydrophobic surface

5.1 Introduction

In this chapter, qualitative features of the evaporation process of small water droplets of base diameter less than 2 millimetres from the same kind of patterned surfaces used in hydrophobicity studies described in section (4.4), partial wetting regimes in section (4.5) and dynamic wetting described in section (4.6) are described. In addition, a quantitive comparison of a diffusion model is performed and estimate of the product of the diffusion constant-water vapour concentration differences are obtained. The patterned surfaces consist of circular pillars (5-15 μm diameter), and centre to centre separation of 20-30 μm. A novel aspect of this study is that the initial contact angle of the drops is very high (in some experiments as high as 154°). Previous experimental studies of evaporation [1-9] dealt with smooth or rough surfaces with initial contact angle less than 120°. To provide data for comparison with evaporation from flat surfaces, flat surfaces were made from the same material as the pillars (SU8-50) and droplets of water deposited on it and the evaporation process was recorded and analyzed.

5.2   Evaporation from flat surfaces

The initial contact angle of water on a flat surface of SU8 is about 80°. Figure
5.1 shows a typical evaporation sequence of a water drop on a flat surface
made from the photoresist Su8-50. In Accordance with previous studies [1],
three phases were observed: in the first phase the base diameter is pinned,
while the contact angle decreases steadily until it reaches what is believed to
be the receding contact angle. In the second phase, the base diameter
decreases, and the contact angle is constant to within 7%. This small variation
in the contact angle might be due to the fact that a perfect flat surface is
difficult to get and all real surfaces are rough to some extent. In the third
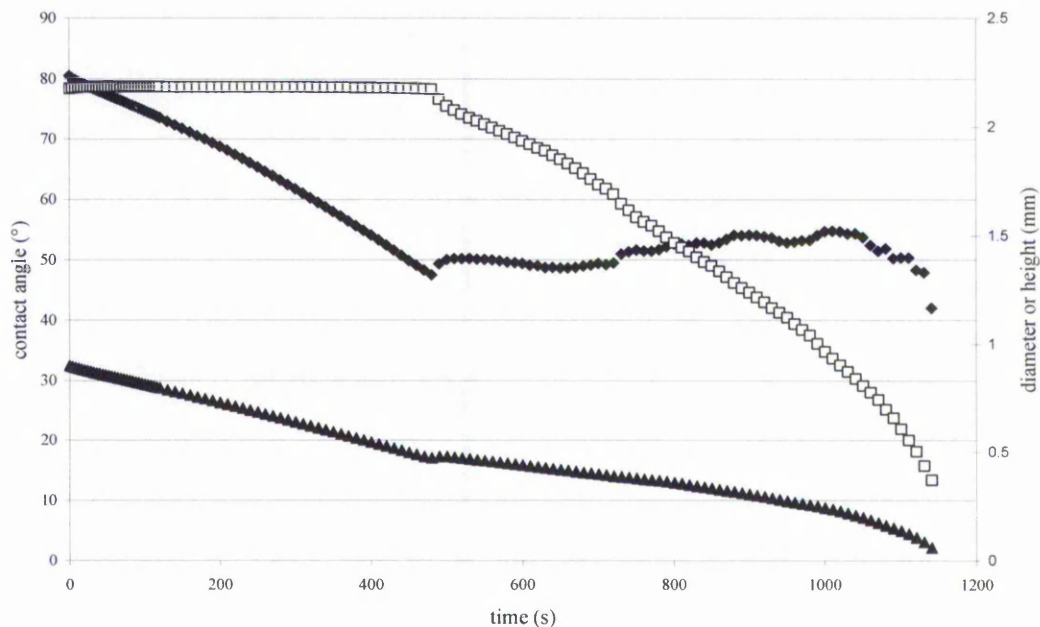phase both the contact angle and the base diameter decrease rapidly.

**Figure 5.1 Evolution with time of the contact angle (♦♦♦) contact diameter (□□□)
and height (▲▲▲) during water droplet evaporation from flat SU8 surface.**

5.3   Evaporation from patterned surfaces

The evaporation pattern follows one of two scenarios, depending on the initial contact angle of the drop which depends on the available energy during deposition on the patterned surfaces [10]. If the drop forms a wetted contact, with the liquid penetrating the patterned surface, then the drop is in a Wenzel state, and the evaporation is dominated by a stage in which the contact line is pinned. The evaporation then proceeds with a contact angle that decreases steadily during the drop life time. On the other hand if the drop forms a composite contact, it is in Cassie state and is characterized by a stick-slip motion. A transition from Cassie Baxter to Wenzel was observed during evaporation of such droplets. In the following sections a description of the evaporation from Wenzel and Cassie-Baxter surfaces are given. As with the spreading of the PDMS oils on patterned surfaces, the figures presented are a selection of a much larger data set.

5.3.1 Evaporation from Cassie surfaces

Gentle deposition of water drop on patterned surfaces of aspect ratio greater than 1 usually results in a drop sitting on a composite (Cassie) surface [11]. The drop doesn't penetrate the patterned surface, which makes it easier for the contact line to move. In the first stage of evaporation the contact line remains pinned and the evaporation results in a decrease of contact angle until it reaches a value believed to be the receding contact angle. Once the contact angle reaches this value no more decrease is allowed, and the drop jumps to the next pillar with a slight increase in the contact angle, avoiding

sinking into the surface structure. The drop then remains pinned for a short while before repeating such a jump (figure 5.2). These jumps referred to as stick-slip motion were also observed in spreading of PDMS oil droplets on the same type of surfaces [12], and are very obvious when watching the video of a drop evaporating from Cassie surfaces.
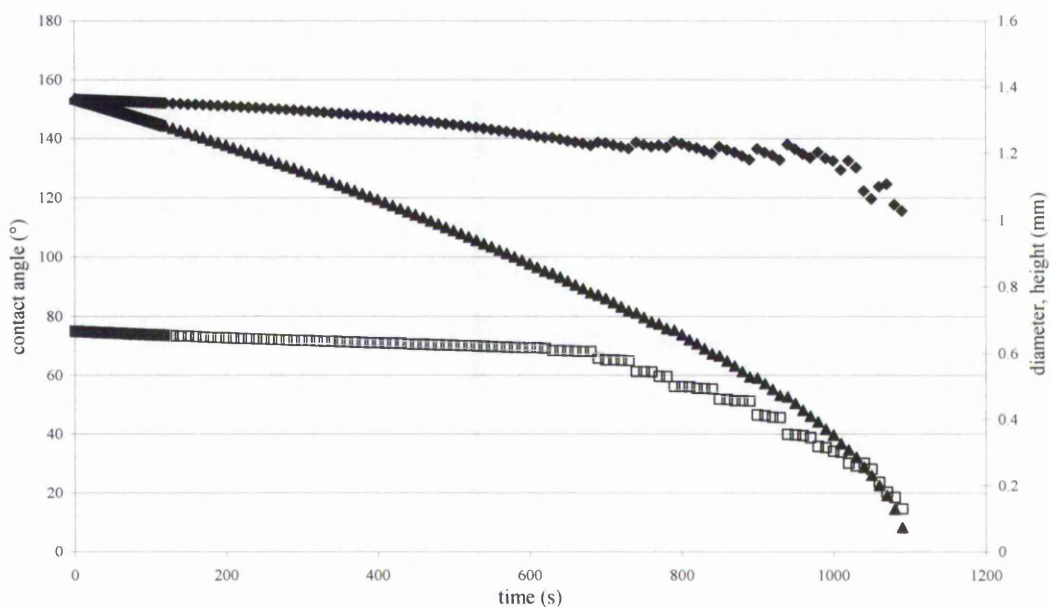

Figure 5.2. Evolution with time of the contact angle (♦♦♦) contact diameter (▲▲▲) and height (□□□) during droplet evaporation from Cassie surface.

A magnified picture of the stick-slip motion was obtained from the evaporation of a large drop (initial volume was 4.61 µL). Figure 5.3 represents the part of the drop life time when the slip-stick motion starts. The centre to centre spacing of the pillars on this surface is 30 µm, the diameter is 8 µm, and its height is 14 µm. The initial contact angle on this surface was 145.6^o. The time period from 2500s to 3100s clearly shows eight steps. During this period the base diameter decreased from 857 µm to 600 µm and this gives average step

of 32 µm compared to the lattice centre to centre spacing, which is 30 µm.
Each step-wise retreat is accompanied by a slight increase in the contact
angle. The explanation could be that the decrease in the contact angle
decreases the outward directed horizontal component of the liquid-vapour
surface tension forces until it reduces to a value that is sufficient to cause this
type of stick slip motion.
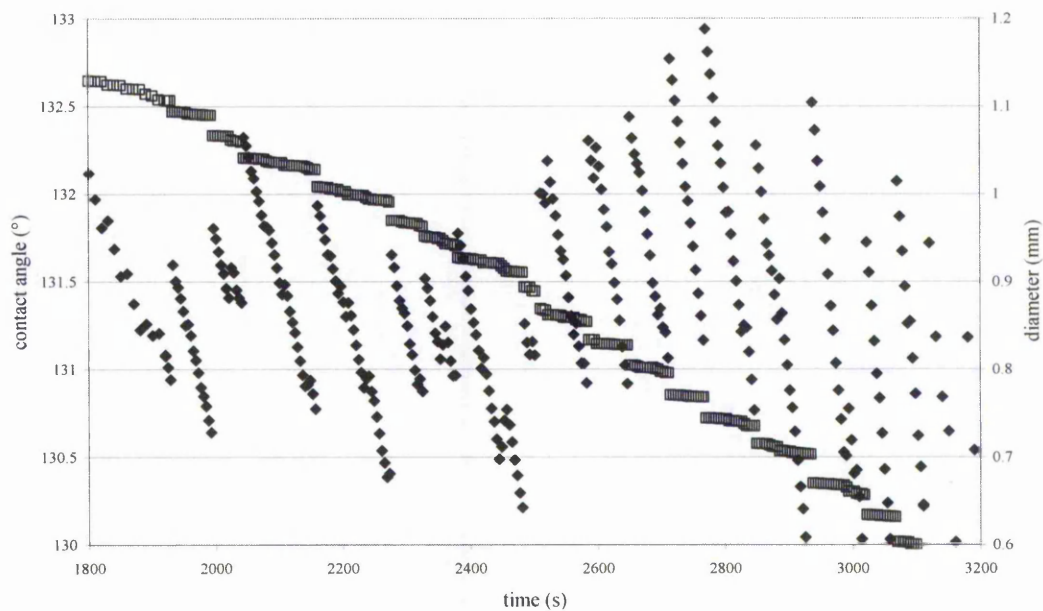
Figure 5.3 Evolution with time of the contact angle (♦♦♦) contact diameter (□□□) during the step wise retreat for a droplet evaporating from Cassie surface.

5.3.2 Evaporation from Wenzel surfaces

Forced deposition of water drop, which is sometimes needed to detach the
drop from the needle, causes it to penetrate the patterned surface i.e. forming
a drop with a wetted contact (Wenzel drop). In this case the contact line is
pinned for most of the drop life time. This pinning causes contact angle
hysteresis, with the contact angle decreasing throughout the whole process of

evaporation. Figure 5.4 shows a typical evaporation sequence of a Wenzel drop. The base diameter remains almost constant during the drop life time except when the drop volume is very small.
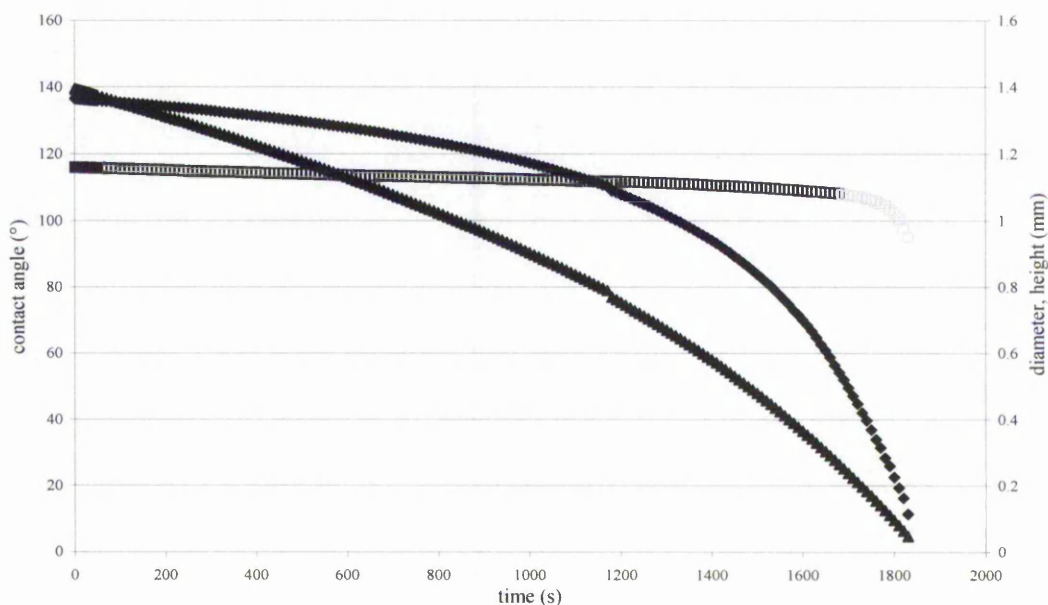
Figure 5.4. Evolution with time of the contact angle (♦♦♦) contact diameter (□□□) and height (▲▲▲) during droplet evaporation from Wenzel surface.

The pinning of the contact line is very obvious in the recorded video for evaporation of (Wenzel drop). The drop remains pinned even when the contact angle drops to a very small value. However the software was not able to determine the value of the contact diameter. The frames presented in figure 5.5 represents the drop late in the evaporation when the contact angle becomes very small and the software becomes unable to determine the value of the contact diameter. On the other hand figure 5.6 represent the drop evaporating from flat surface, with the contact diameter decreasing i. e. there is no contact line pinning.

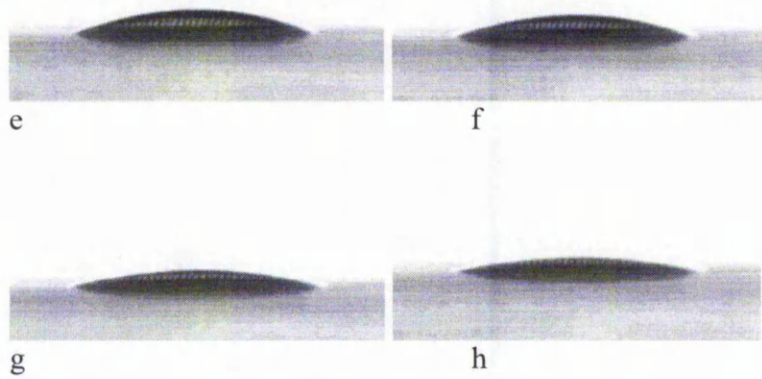**Figure 5.5. A Wenzel drop late in the evaporation. The drop contact angle decrease from e to h while the contact diameter remains pinned as the drop volume decrease.**
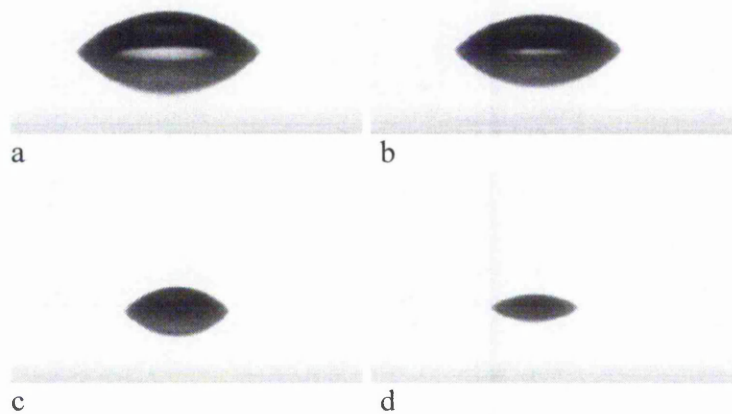

Figure 5.6. Drop evaporating from flat surface. Both of the contact angle and contact diameter decrease as the drop volume decrease from a to d.

5.3.3 Transition from Cassie to Wenzel

A transition from Cassie-Baxter to Wenzel regime was observed. This transition or drop collapse occurred during deposition, shortly after drop deposition (within few seconds) or a long time after the deposition. Figure (5.5) shows two drops evaporating. The first (figure 5.5 a to d) collapses after about 14 minutes. The second drop (figure (5.5 e to h) collapses only when the drop volume becomes too small.
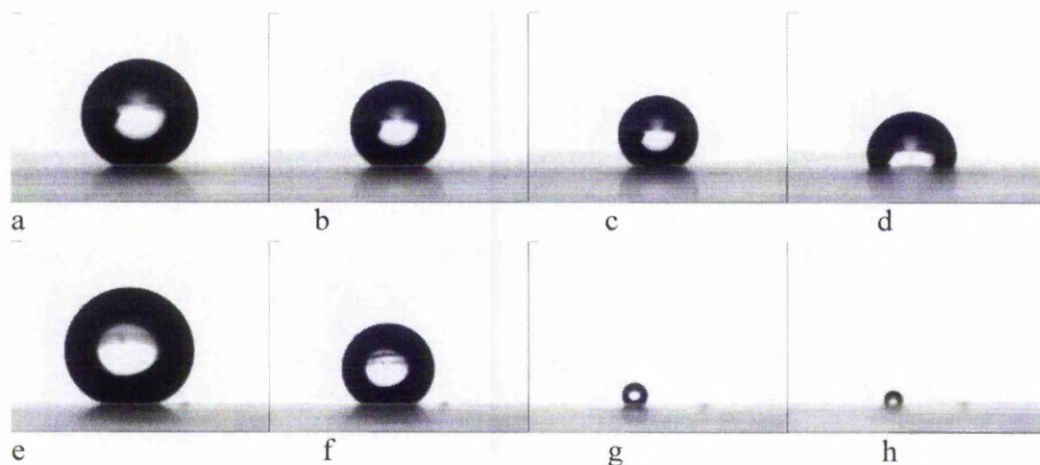
Figure (5.7) transition from Cassie to Wenzel can occur either in the middle of the evaporation process (c to d present drop collapse in one frame, which is less than one second) or late in the evaporation (g to h, the time difference between them is 20 seconds, but due to resolution problems the moment the drop collapsed could not be determined). The magnification has not been changed during the evaporation.

It is believed that all drops change to Wenzel regime late in the evaporation process. This was not determined due to the resolution of the experimental system.

Figure 5.8. Evolution with time of the contact angle (♦♦♦) contact diameter (□□□) and height (▲▲▲) for a drop that collapsed during evaporation. The data correspond to figure 5.5, a to d.

5.4   Evaporation and hysteresis

Evaporation causes the drop to recede due to volume reduction. Drop receding results in a new value of the contact angle. This causes existence of a range of apparent contact angle on the surface (i. e. hysteresis). In the evaporation experiments two scenarios were observed with different hy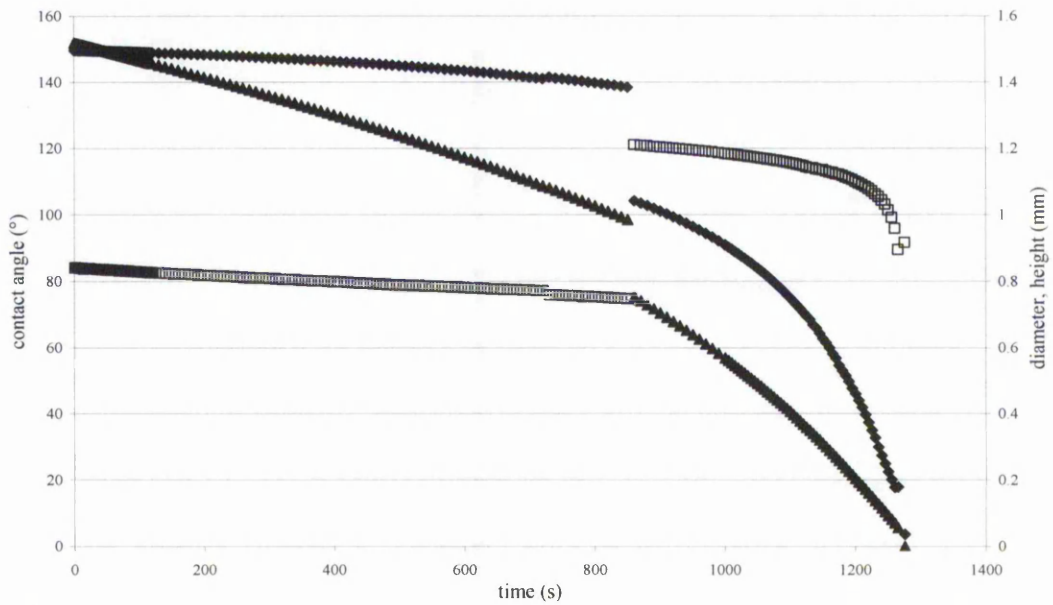steresis behaviour. The first is the hysteresis of a Wenzel drop, which is very large. The receding angle kept decreasing, and couldn't be measured when the drop volume became very small (about 0.01µL). In accordance with results obtained by Patankar *et al* [13], (who measured the receding contact angle by withdrawing liquid from the drop using an a utomatic dispensing syringe), no conclusion about the value of the receding angle was drawn because the drop becomes too small to analyze.

On the other hand a Cassie drop shows a much smaller degree of hysteresis. In the particular example shown in figure 5.2, the hysteresis is about 15° (the difference between the initial contact angle and the contact angle just before the drop starts jumping) . The obvious stick-slip motion of the drop, which starts when the drop reaches the minimum receding angle, is a very interesting behaviour in its own, since it is motion on horizontal surfaces caused by the surface tension forces.

5.5   Diffusion constant-vapour concentration difference (DΔc)

In Chapter 2 a model for evaporation of droplets from surfaces based upon diffusion into the surrounding space was presented; this model also allows the calculation of the diffusion constant-vapour concentration difference product of vapour into the air (See also ref [14]). The model is valid for drops of initial contact angle greater than 90° in the mode characterized by contact line pinning up to the moment the drop contact angle become less than 90° (in the Wenzel case), or the start the step wise retreat (in the Cassie case), or a collapse over the surface structure occurs (undergoes transition from Cassie to Wenzel state).

For determining the diffusion coefficient-concentration difference product, the two equations (2.51) and (2.56) are rearranged into forms which predict straight-line graphs:

$$\frac{\rho r_b^2}{2} H_{PB}(\theta) = -D\Delta ct + k_1 \qquad (5.1)$$

And $\dfrac{\rho A_{lv}}{8\pi f_{ave}} = -D\Delta ct + k_2$ (5.2)

Figure 5.9 shows equations (5.1) and (5.2) calculated from the data for θ, r_b and A_{lv}, which corresponds to the same experiments presented in figure 5.2 (lower pair of curve), figure 5.4 middle pair of curves and figure 5.3 upper pair of curve.

The average of the initial and the final values has been used for f_{ave}. The solid curves are straight line fits over the range before either the drop collapse or starts stepwise retreat (lower and middle 2 curves) or reaches 90° (upper 2 curves). The fits show excellent agreement with the expected linearity having R^2 parameters better than 0.9999, although equation (5.1) gives a slightly higher estimate than equation (5.2) for the diffusion constant/vapour concentration difference product ($D\Delta c$).
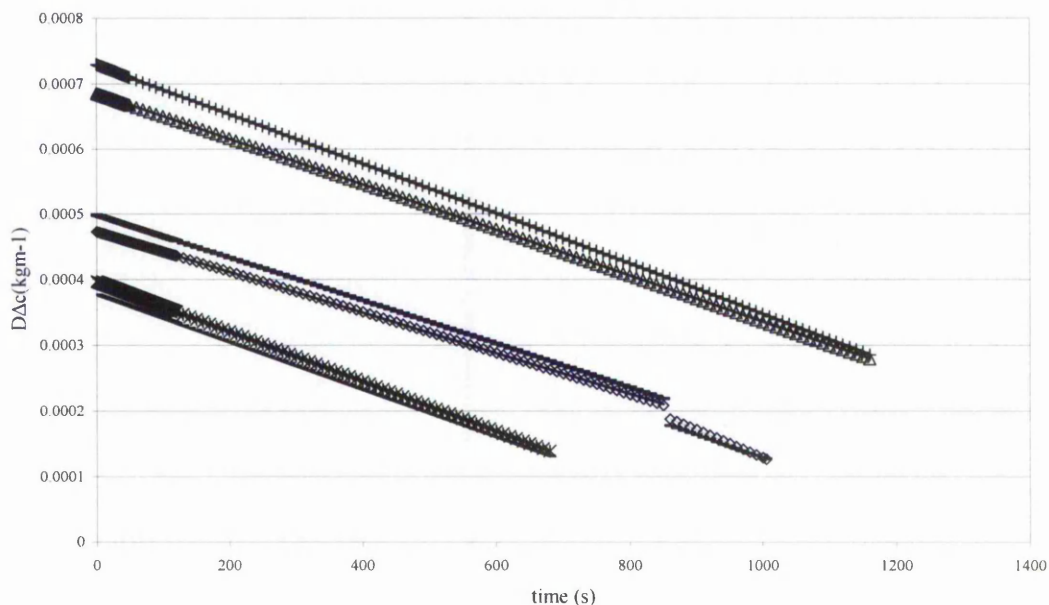
Figure (5.9) Tests of equation (5.1) and equation (5.2) for the data in figure (5.2) (lower pairs of curves), figure (5.8) (middle pair of curves) and figure (5.4) (upper pair of curves). The solid lines are fits over the range to when the drop contact angle becomes 90 (upper pair), collapse (middle pair) or start the stepwise retreat (lower pair). The data of the upper pair of curves was multiplied by 1.5 to avoid intersection with the middle pair curves data.

5.6 Diffusion constant

The diffusion constant was determined for a number of experiments carried out on two surfaces: surface A with pillars diameter of 10 μm and centre to centre separation of 20 μm and surface B with pillars diameter of 10 μm and centre to centre separation of 30 μm; the results are displayed in table (5.1). The data used for calculating the diffusion coefficient corresponds to constant base diameter (which is taken to be data within 4% of its initial value) and contact angle greater than 90°. The fits of the two equations (5.1) and (5.2) to

the data were straight lines with regression coefficient parameters better than R=0.9999. The calculated diffusion coefficient was compared to values from the CRC Handbook, which gives a value of $2.39 \times 10^{-5} \, m^2 \, s^{-1}$ at 8°C. This value was used to calculate the diffusion constant at the experimental temperature using a $T^{3/2}$ temperature dependence relation. The results were within a few percent of these reference values indicating a successful model.

Surface	T (C°)	RH (%)	Δc (g m⁻³)	θ_i	θ_f	$D\Delta c$ (x10⁻⁷ kg m⁻¹s⁻¹)		D (x10⁻⁵ m⁻²s⁻¹)		
						Eq (5.1)	Eq (5.2)	Eq (5.1)	Eq (5.2)	Ref. value
A	23	58	8.62	133.3	106.3	2.396	2.358	2.780	2.735	2.584
A	24	57	9.34	136.6	103.1	2.559	2.481	2.740	2.657	2.597
A	26	57	10.45	140	94.8	2.961	2.588	2.833	2.476	2.623
A	26	47.5	12.76	136.2	92.3	3.258	3.189	2.553	2.499	2.623
B	23	51	10.06	125.9	90.6	2.664	2.588	2.648	2.572	2.584
B	23	51	10.6	141.3	129.5	2.714	2.399	2.698	2.385	2.584
B	25	48.3	11.88	125	90.3	3.194	3.153	2.688	2.654	2.610
B	26	46	13.12	138.9	118.4	3.318	3.068	2.529	2.339	2.623

Table 5.1. Estimate of diffusion coefficient for water into air for droplets on two SU-8 50 surfaces: Surface A with 10μm-diameter pillars separated by 10μm and surface B with 10 μm-diameter pillars separated by 20μm.

In this chapter the evaporation of water droplets from hydrophobic and superhydrophobic surfaces has been studied. Two possible drop configurations were observed on the same patterned surface. The first corresponds to the Wenzel and the second to the Cassie-Baxter state. Each has a different evaporation pattern. The main difference between the two cases is contact line pinning, which influences the pattern of evaporation, and is observed in both of the Wenzel and Cassie case, but for a much shorter time in the Wenzel state. The evaporation in a Wenzel state is characterized by contact line pinning for more than 90% of the drop life time. On the other hand the evaporation from Cassie surfaces is characterized by stick-slip motion. The interesting thing about this motion is that it is a motion on horizontal surfaces driven by the surface tension forces and evaporation. Diffusion constant calculated from the drop profile evolution with time has shown to be within eight percent of the values from the reference handbook (15).

References

1. R. G. Picknett, R. Bexon, *Journal of Colloid and Interface Science,* **1977**, *61,* 336

2. K. S. Birdi, D. T. Vu, A. Winter, *Journal of Physical Chemistry,* **1989**, *93,* 3702.

3. Birdi, K. S.; Vu, D. T. *Journal of Adhesion and Science Technology,* **1993**, *7,* 485.

4. M. E. R. Shanahan, C. Bourgès, *Int. J. Adhes. Adhes.,* **1994**, *14* (3), 201.

5. C. Bourgès-Monnier, M. E. R Shanahan, *Langmuir,* **1995**, *11,* 2820.

6. S. M. Rowan, M. I. Newton, G. McHale, *Journal of Physical Chemistry,* **1995**, *99,* 13268.

7. S. M. Rowan, G. McHale, M. I. Newton, M. Toorneman, *Journal of Physical Chemistry,* **1997**, *101,* 1265.

8. G. McHale, S. M. Rowan, M. I. Newton, M. K. Banerjee, *Journal of Physical Chemistry B,* **1998**, *102,* 1964.

9. H. Y. Erbil, G. McHale, M. I. Newton, *Langmuir,* **2002**, *18,* 2636

10. N. A. Patankar, *Langmuir,* **2003**, *19,* 1245.

11. N. J. Shirtcliffe, S. Aqil, C. Evans, G. McHale, M. I. Newton, C. C. Perry, P. Roach, . *Journal of Micromechanics and Microengineering,* **2004**, *14,* 1384-1389.

12. G. McHale, N. J. Shirtcliffe, S. Aqil, C. C. Perry, M. I. Newton, *Physical Review Letter* **2004**, *93,* article 036102.

13. B. He, J. Lee, N. A. Patankar, *Colloids and surfaces A: physiochemical Engineering Aspect*, **2004**, *248.*

14. G. McHale , S. Aqil, N. J. Shirtcliffe, M. I. Newton, H. Y. Erbil, *Langmuir,* **2005**, *21,* 11053.

15. R. C. Weast, M. J. Astle, CRC Handbook of Chemistry and Physics, 62nd ed.: *CRC Press*: Boca Raton. FL, 1981-1982.

Chapter 6

Conclusion

6.1 Conclusions

In this thesis photolithography using a thick-film photoresist SU-8 50 has been developed as a reliable and reproducible technique for fabrication of microstructured patterned surfaces for studies of wetting. The patterned surfaces obtained were cylindrical pillars of diameter ranges between 4 and 40 μm with relatively high aspect ratio (sometimes greater than 4). These microstructured patterned surfaces have been used to investigate super-hydrophobicity and spreading of liquids. Such work may benefit many industries, such as those interested in self cleaning surfaces and manipulation and guiding of drops motion in microfluidic systems.

The equilibrium contact angle for water droplets on the photoresist surfaces has been shown to be a function of the pattern dimensions. The height of the pillars determines whether Wenzel or Cassie type droplets will form. Beyond a unity aspect ratio, the most probable drop configuration corresponds to Cassie provided that the drop is deposited gently. Multiple equilibrium droplet configurations (Wenzel and Cassie with wetted and composite contacts, respectively) were observed on the patterned surfaces. A transition from a Cassie state to a Wenzel state was reported during drop deposition.

In the early part of the thesis the effect of patterned substrates on water repellency was the focus of the work. Subsequently, surface patterns were shown to alter the speed of spreading of other liquids, such as oils, on the

surfaces. The contact angle–time relation, for completely spreading and non-volatile liquids, was shown experimentally to follow a power law with a higher exponent for the patterned surface than the flat one. The drop edge speed tends to a linear function in the dynamic contact angle instead of a cubic function as on a flat surface. This effect could be of benefit to the coating and lubrication industries. A better understanding of the spreading dynamics is also relevant to oil decontamination.

Many liquids, including water, are volatile and unless the surrounding vapour is entirely saturated, evaporation will occur. In the final part of this thesis a description of the two possible patterns of evaporation of sessile droplets from hydrophobic and superhydrophobic surfaces was given. This comprised the evaporation from the surface by a droplet with a completely wetted contact (Wenzel state) and the evaporation from a surface by a droplet possessing a composite contact (Cassie state). The contact line pinning mode in Wenzel state evaporation occupies more than 90% of the drop life time. On the other hand in the Cassie state evaporation, the contact line pinning terminates the moment the contact angle reaches the minimum receding angle and at that time the drop begins a step wise retreat which mirrors the underlying lattice structure. The diffusion constant-vapour concentration difference product (i.e. DΔc) was calculated and an estimate of the diffusion coefficient obtained.

6.2 Future work

There are many areas were further investigation could be done either using the type of model surface developed in this thesis or to further study physical effects related to topography and wetting. The following areas may be of interest.

Spreading on micro-structured surfaces. This thesis reports about macroscopic spreading on structured/patterned surfaces caused by surface tension forces and Laplace pressure across a curved interface. However the precursor film spreading (which is caused by the long range van der Waal's forces) was not investigated. Doing so would provide a better insight into the spreading mechanisms and dynamics as droplets entered a film regime.

Contact angle hysteresis of Cassie drops.   The effect of drop volume on contact angle hysteresis on microstructured surfaces has not been investigated. One method of measuring hysteresis (of a Cassie type drop) is by tilting the substrate up to the moment the drop begins to move. It has been observed that small drops (of sizes less than 1.5 μL) do not move even when the substrate is tilted vertically. This means that smaller drops require stronger forces to actuate motion. This depends on the initial contact angle, and therefore a study aiming to relate the initial contact angle of a Cassie drop to the force require to move droplets of small sizes across surfaces is needed. This would benefit microfluidics applications.

Evaporation from superhydrophobic surfaces: A transition from a Cassie to Wenzel state during evaporation was observed. However, the precise conditions triggering the Cassie to Wenzel transition was not studied. Also whether heat flow from the substrate influenced evaporative cooling, and if so, whether this would be changed due to the different microscopic contact area between a micro structured solid surface and Cassie type drop. It may be possible to relate drop evaporation from Cassie type surfaces (where the drop sits on a solid –vapour surface) to the Leidenfrost effect in which a layer of vapour prevents heat transmission and hence reduces evaporation. Since superhydrophobic surfaces are common in nature and the conservation of water droplets or vapour near the leaves of plants is of importance, further study of evaporation from a superhydrophobic surface could have relevance to biological systems as much as physical systems involving heat and mass transfer.